INSTITUTO POLITÉCNICO DE BRAGANÇA Escola Superior de Tecnologia e Gestão

UNIVERSIDADE TECNOLÓGICA FEDERAL DO PARANÁ

Electromagnetic Modeling Approaches of Static Electric Machines

KATHLEEN CAROLINA DE MORAIS DE CARVALHO

Supervised by

Prof. Dr. Ângela Paula Ferreira

Prof. Dr. Ednei Luiz Miotto

Bragança

2019/2020

INSTITUTO POLITÉCNICO DE BRAGANÇA Escola Superior de Tecnologia e Gestão

UNIVERSIDADE TECNOLÓGICA FEDERAL DO PARANÁ

Electromagnetic Modeling Approaches of Static Electric Machines

KATHLEEN CAROLINA DE MORAIS DE CARVALHO

Thesis presented in the School of Technology and Management of the Polytechnic Institute of Bragança to fulfill the requirements of a Master of Science Degree in Industrial Engineering (Electrical Engineering branch).

Supervised by

Prof. Dr. Ângela Paula Ferreira

Prof. Dr. Ednei Luiz Miotto

Bragança

2019/2020

To my greatest example of engineer,
my father.

Acknowledgments

Primarily I would like to thank my advisor Prof. Drª Ângela Paula Ferreira for the opportunity to work in the amazing field of electric machines during my master's degree, for all support, by criticisms, advices and reviews. I also would like to thank to Prof. Dr. Ednei Luiz Miotto for all support during the writing process, and Prof. MA Marilice Zavagli Marson for all fast reviews and the emotional support during all process.

I am profoundly grateful to my family, which always support my dreams, cheer for all my accomplishments and believe in my potential since the beginning, especially my parents, Renata Aparecida de Morais de Carvalho e Guilherme de Carvalho.

I would like to thank my boyfriend Nícolas Pape for staying by my side despite the distance, encouraging me and being my best friend during the most difficult period of my academic life.

My special thanks for Prof. Dr. Alessandro Goedtel who gave me the opportunity to work in Intelligent Systems Laboratory during my graduation, and is an example of professional.

Finally, my special tanks to all professors that I had in my entire life and contribute to my academic development, especially Prof. MA Roberto Bonato who told me to not study medicine and being an engineer, thank you very much.

Abstract

The efficiency improvement of electric machines of major importance in the industrial field, considering that those devices represent a large portion of electricity consumption. Therefore, in the study of electromagnetic projects is mandatory to analyze the behavior of electric devices in rated and exceptional operation conditions. In this context, the application of the finite element method is relevant, since its high degree of discretization allows to analyze fields distribution with an accuracy not obtained by analytical approaches. When applied to complex domains, such as electric machines, that method makes it possible to verify saturation points and active losses in the device, with high accuracy.

Thereby, this work proposes a computational model of a single-phase E-core transformer, assisted by the finite element method. The project is based on three approaches, in order to stablish a comparative analysis among the outputs.

First of all, was analytically calculated through a reluctance mesh able to verify the magnetic flux distribution in the middle path of the transformer's core. For this purpose, the project of the windings was necessary, based on the stablished physical characteristics and electric parameters.

The second approach was the design the computational model, considered a 2D approach, to evaluate magnetic magnitudes, also calculated by the reluctance network. On the other hand, the 3D model was developed in order to evaluate the losses distribution around the whole volume of the domain. The proposed models were evaluated in a static, by reluctance mesh and the computational model, and time-varying domain, in order to analyze the losses.

Finally, a physical prototype was also tested, at no-load and short-circuit tests, to provide data about the transformer losses under rating conditions. Those results were used to validate the efficiency of the computational model to predict the core and resistive losses.

Keywords: Transformer; Finite element method; Losses; Prototype.

Resumo

O melhoramento da eficiência de máquinas elétricas é de grande importância para o setor industrial, uma vez que estes equipamentos representam uma ampla porção do consumo de eletricidade. Desta forma, o estudo de campos eletromagnéticos é essencial para analisar o comportamento de equipamentos elétricos em condições de operação nominais e excepcionais. Neste contexto insere-se a relevância do método dos elementos finitos, em virtude de análises de distribuição de campos com um alto grau de discretização não obtido através de abordagens analíticas. Quando aplicado a domínios complexos, como, por exemplo, máquinas elétricas, este método permite verificar pontos de saturação e perdas acerca de todo o domínio, com alta precisão.

Deste modo, o presente trabalho propõe um modelo computacional de um transformador monofásico de núcleo envolvente, assistido pelo método dos elementos finitos. O projeto é baseado em três abordagens, a fim de estabelecer uma análise comparativa dos resultados.

Primeiramente, foi o calculada analiticamente uma rede de relutâncias capaz de verificar a distribuição do campo magnético no caminho médio do núcleo do transformador. Para isso, fora necessário o projeto dos enrolamentos, baseados nas características físicas e parâmetros elétricos estabelecidos.

A segunda abordagem consistiu no design do modelo computacional considera uma abordagem 2D para validar grandezas magnéticas, também calculadas pela rede de relutâncias. Por outro lado, o modelo 3D foi desenvolvido a fim de avalizar a distribuição de perdas em todo o volume do domínio. Os modelos propostos foram avaliados em domínios estáticos, pela rede de relutâncias e pelo modelo computacional, e variantes no tempo, para a análise de perdas.

Por último, um protótipo físico também foi testado, de forma que os testes a vazio e de curto-circuito fornecessem dados referentes às perdas no transformador operando em condições nominais. Esses resultados foram utilizados para a validação da eficiência do modelo computacional na previsão de perdas no núcleo e resistivas.

Palavras-chave: Transformador; Método de elementos finitos; perdas; protótipo.

Contents

List of tables

List of figures

Acronyms

2D	Two-dimension
3D	Three-dimension
AC	Alternating current
AWG	American wire gauge
DC	Direct current
FE	Finite Element
HV	High voltage
IEC	International Electrotechinal Commission
LV	Low voltage
PDE	Partial Differential Equation

List of symbols

$\boldsymbol{A}$	Magnetic potential field vector
A_s	Sectional area
$\boldsymbol{B}$	Magnetic flux density
$\boldsymbol{B_m}$	Maximum magnetic flux density
$\boldsymbol{B_r}$	Residual magnetization
$\boldsymbol{D}$	Electric flux density
D	Domain
d	Thickness of lamination sheets
dl	Differential close path
d_S	Differential space
$\boldsymbol{E}$	Electric field
$F(\varphi)$	Minimizing function
f	Frequency
f	Known function defined
$\mathscr{F}$	Magnetomotive force
$\mathscr{F}_{HV}$	High voltage magnetomotive force
$\mathscr{F}_{LV}$	Low voltage magnetomotive force
$\boldsymbol{H}$	Magnetic field
$\boldsymbol{H_c}$	Coercive magnetic field
I	Current
$\boldsymbol{J}$	Current density
J_z	Current density (z axis)
k_c	Eddy-current loss coefficient
k_e	Excess loss coefficient
k_h	Hysteresis loss coefficient
L	Differential operator

l	Length of magnetic flux middle path
$\boldsymbol{M}$	Magnetization vector
N	Number of turns
$\boldsymbol{P}$	Polarization vector
P_j	Resistive loss
P_s	Power supplied
P_{str}	Stray losses
R	Resistance
R_i	Residual integral
$\mathscr{R}$	Reluctance
$\mathscr{R}c$	Central reluctance
$\mathscr{R}s$	External reluctance
r	Defined space (x, y, z)
t	Time
V	Voltage
V	Electric scalar potential
V_{rms}	
v_j	Expansion function
w_i	Weight function
ε	Electrical permeability
ε_0	Electrical permittivity (vacuum)
ε_r	Relative permittivity
θ_j	Coefficients
μ	Magnetic permeability
μ_0	Magnetic permeability (vacuum)
μ_r	Relative permeability
ρ	Volume charge density
σ	Conductivity
τ_D	Domain volume
Φ	Magnetic flux
φ	Function
φ^*	Approximate function

χ_e Electric susceptivity

χ_m Magnetic susceptivity

Chapter 1

1 Introduction

1.1 Work motivation

The present work intents to report a study of electromagnetic model of static electric machine, based on an analytical model and the numerical method of Finite Element (FE).

Inside this context where all the physical phenomena are described by differential equations, usually complicated to be solved by classical analytical methods, a numerical analysis based on FE method allows a higher discretization of flux distribution [1]. In the case of electromagnetic analyses the numerical models are based on the determination of distribution electric and magnetic fields, by solving Maxwell's equations subjected to given boundary conditions [1]–[3].

The FE method was proposed in 1940's, but only after a decade of studies started to be use in aeronautical design and structural analyses. With the advance of computational technologies in 1970's the method started be used to solve problems related to electromagnetism. In current days, the finite element method is the most spreaded method to solve vector field problems [2]–[5].

Due to the limitation of analytical methods to objects with simple geometry, and the necessity of rigorous solution with high degree of discretization of electromagnetic fields study, the use of the FE mathematical tool improved the development of projects and reduced the number of physical prototypes to laboratorial tests [1], [3], [5]–[7].

The focus of this work is analyzing the behavior of a low power single-phase E-core transformer, using the FE method and compare the predict of losses, by the method, to outputs

of experimental tests, from a physical prototype. The selected software to the development of project was *ANSYS*®, Maxwell package for the range of tools to electromagnetic analyses.

1.2 Study case: single-phase transformer

The electric machine chosen to be modeled and analyzed is a low power single-phase transformer. This selection was made by convenience due to the possibility to validate the outputs from the FE method to experimental results from a physical prototype and for the sake of simplicity associated to static machine.

A transformer is an electric device invented in the end of 19th century with a work principle based on Faraday's law, in which a changing magnetic flux, Φ, through a wire loop, in this case a coil, induces a voltage, V, proportional to the number of winding's turns, N, with polarity defined by Lenz' law, [3], [8]–[11], as follows.

$$V = -N\frac{d\Phi}{dt} \tag{1.1}$$

The transformer has an important role in the electrical system, since this device allows de reduction of Joule effect in transmission and distribution, by the increase of the voltage, decreasing the current and consequently reducing the resistive loss. Also, allows the connection of a range of equipment, with different voltages levels at the same grid [12].

A transformer project is based on the physical modeling and components features definition, like the material of core and windings. Those setups determine the machine behavior in different working situations. In this context the main task is setting the core material features, since it is necessary to introduce saturation effects, hysteresis and eddy-current losses, as well as the core topology according to windings configuration [11], [13].

1.2.1 Electric parameters

The core topology chosen for the transformer under analysis is an E-core, also called shell type. In this type of transformer, the windings are overlapped and the core edges wrap those coils, improving the coupling and, consequently, reducing the value of a leakage flux [12]. This topology is more efficient than the core type, and its design and dimensions, to this project, are shown in Figure 1-1.

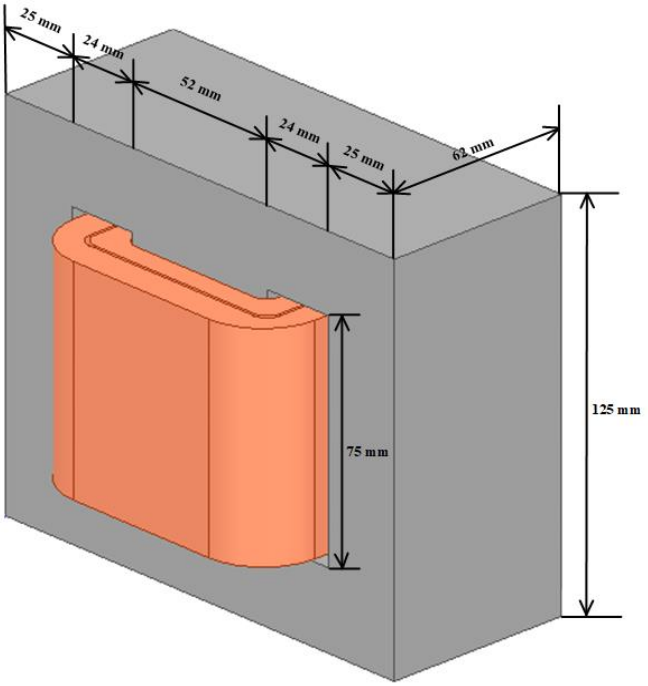

Figure 1-1. Transformer dimensions.

The transformer's electric project was based on a standard frequency of 50 Hz, power rating of 1000 VA and voltage ration of 220/110 V. With those technical characteristics and the available space for the copper winding, the wire gauge involved has a diameter of 1.45 mm to high voltage winding and 2.05 mm to low voltage winding, considering the rated currents required. The estimative calculation of windings resistances is presented on Appendix A.

1.2.2 Core characterization

Soft ferromagnetic materials are required as core material, because of the facility to drive flux from one point to another, and their power loss are proportional to the area of the hysteresis loop, that should be as smaller as possible [14]. The structure of the core is an arrangement of laminated sheets, insulated from each other to reduce the induction of eddy-current losses.

The hysteresis loop characterize the behavior of ferromagnetic material, when an external magnetic field is applied on it, as proposed in Figure 1-2.

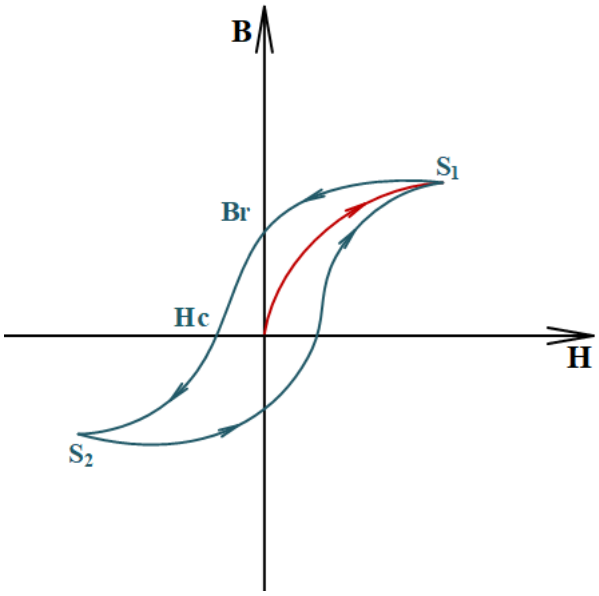

Figure 1-2. Hysteresis loop.

The red curve represents the first magnetization of the material, in which the magnetic flux density (***B***) increases according to the magnetic field (***H***), but not with a linear behavior. When the curve reaches the horizontal behavior, the material saturates, represented by the points S_1 and S_2. The gradual reduction of ***H*** does not have an equivalent decrease of ***B***. Therefore, with ***H*** equal zero in the demagnetization, the material has a residual magnetization, named by $\boldsymbol{B_r}$. With ***H*** in the opposite direction, ***B*** decreases until zero, until the point of coercive magnetic field $\boldsymbol{H_c}$. The loop is completed when ***H***, in the opposite direction, is reduced to zero and increases in a magnetization direction until S_1 [14]–[17].

In the experimental prototype used for validation purposes, the magnetic features of iron core are unknown, therefore, the magnetization curve used to model the device by FE method is assumed as the one shown in Figure 1-3, and the power loss curve is displayed in Figure 1-4.

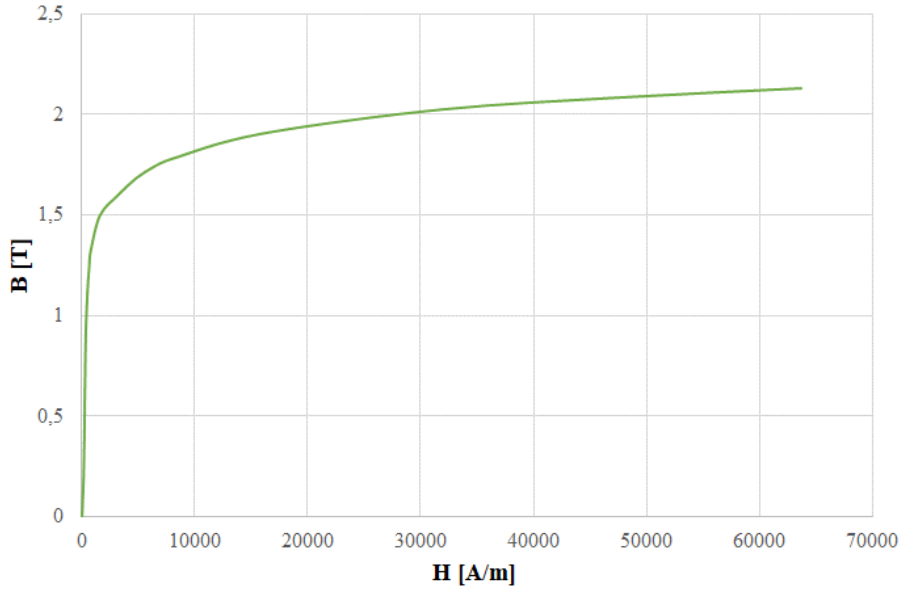

Figure 1-3. Magnetization function. Adapted from [18].

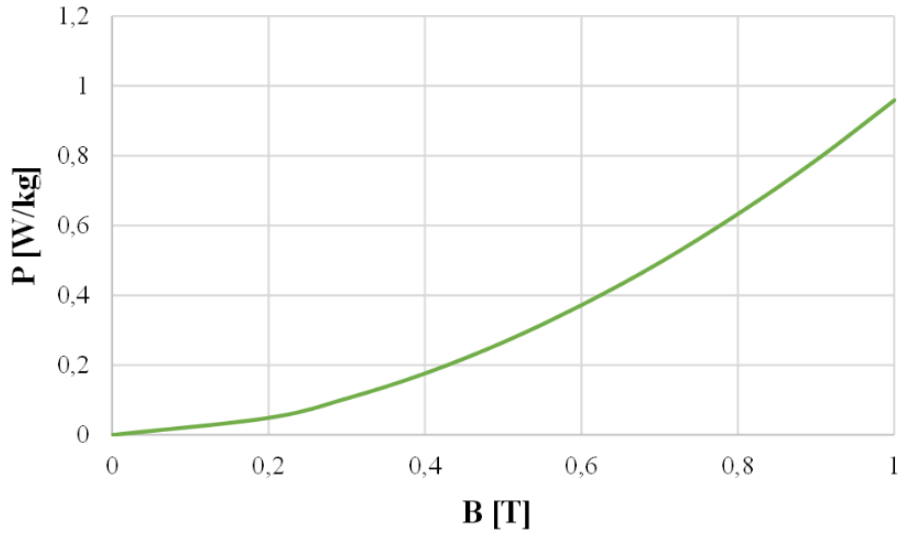

Figure 1-4. B-P curve. Adapted from [18].

1.3 Objectives

The main goal proposed by this dissertation is modelling and evaluate a design of a single-phase transformer by the finite element method to predict power losses in no-load and rating operations. With this purpose, the specific objectives of this work are given by:

- Development of analytical project of magnetic magnitudes, based on reluctance network theory;
- Design of numerical model able to predict power losses with high degree of discretization;

- Characterization of a consistent physical prototype to computational prototype able to provide experimental outputs, with comparative purposes.

1.4 Work structure

This work is structures as follows:

- Chapter 1: Introduction

  Description of the work motivation, followed by the characterization of the study case and the objectives of the present dissertation.

- Chapter 2: State of the art

  Literature review of finite element method applied to electromagnetic problems, description of the tool, history and a review about similar works.

- Chapter 3: Review of electromagnetics and power losses
  - Literature review of Maxwell's equations in magnetostatic and sinusoidal time domain variation;
  - Review of transformer power losses: core, resistive and stray losses.

- Chapter 4: Analytical electromagnetic design approach
  Analytical project based on reluctance network and analysis of magnetic flux in a 2D approach.

- Chapter 5: Finite element method design approach

  Numerical analysis, geometry simplification, solution type, boundary condition, partition of the domain and postprocessing.

- Chapter 6: Results and discussions
  Introduction of experimental prototype, and comparative analyses of numerical outputs, analytical approach and experimental results.

- Chapter 7: Conclusion
  Final contents and recommendations to future works.

Chapter 2

2 State of the art

2.1 Fundamentals of the finite element method

All physical phenomena are modeled by integral or partial differential equations, being the numerical technique of finite element method suitable to predict the behavior of a range of objects. The main advantage of the method is due to the fact of classical analytical methods being too complicated to solve those problems in a complex geometry. Thereby, this numerical approach allows a higher degree of discretization of differential equations solution which can be solved by an approximate manner [1], [3].

The base algorithm used to formulate and solve a mathematical problem using the method consists of three steps. First of all, in the preprocess are set the geometry, boundary conditions, and the problem is formulated by the partial differential equations. In the second stage the domain under analysis is divided in a great number of smaller subdomains connected by nodes, which compound the finite mesh. The last stage, called postprocess, encompass analyses of field overlays, 2D and 3D reports plot, fields calculator, output variables and design summary [1]–[3], [19].

The linear equation system that compose the finite element mesh, is associated to boundary conditions stablished by methods used to formulate integro-differential equations with boundary conditions applied in each subdomain. The two major methods used in this formulation process are the classical residual method, recognized as Galerkin's method and the classical variational method, called Rayleigh-Ritz's method [2], [20].

These two methods intent to define a function φ^* (Eq. 2.1) that approximates as close as possible to function φ, which is the description of the vector field problem by the application of a differential operator (L), in a domain D [2], [3], [20], given by,

$$\varphi^*(r,t) = \sum_{j=1}^{N} \theta_j v_j(r,t) \tag{2.1}$$

$$L\varphi(r,t) = f(r,t) \tag{2.2}$$

where θ_j are unknown coefficients, v_j is expansion function, f a known function defined in space $r = (x, y, z)$ and time, t.

2.1.1 The Rayleigh-Ritz's method

The variational method solves field problems by an integral approach and is formulated in terms of a variational expression, from a differential equation, of which the minimum corresponds to the solution of the field problem under given boundary conditions. The approximate solution is obtained by minimizing the function with regard to variables. The minimizing function proposed by the method is shown in Equation (2.3) [2], [3].

$$F(\varphi) = \frac{1}{2}\langle L\varphi, \varphi\rangle - \frac{1}{2}\langle \varphi, f\rangle - \frac{1}{2}\langle f, \varphi\rangle \tag{2.3}$$

2.1.2 The Galerkin's method

In the classical residual method, as the name indicate, the field problem solution is based on reducing the residual of differential equations. Assuming that function φ^* is a better approach to the exact function φ (Eq. 2.2), the residual is given by Equation (2.4) and must be nearly to zero [2], [3].

$$r^* = L\varphi^* - f \neq 0 \tag{2.4}$$

To the best approximation of function φ^*, the Garlekin's method enforce the follow conditions

$$R_i = \int_{\tau_D} w_i r^* \, d\tau = 0 \tag{2.5}$$

being the weighted residual integral (Ri) formulated by weight function (w_i) and the domain volume (τ_D). The weight functions are chosen equal to interpolation functions (v_i) to more accurate solutions:

$$w_i = v_i \qquad i = 1, 2, 3, \ldots, N \qquad (2.6)$$

The tool chosen to this work used to apply the finite element method is the commercial software ANSYS®, Maxwell's package, whose formulation is based on Galerkin's method [21].

2.2 History

The finite element method does not have only one creator, since this type of analysis came from two fields, the mathematic and engineering. The first register of differential equations in a surface with minimum area bounded by a closed curve in space was in 1851, with Schellbach's study, which discretizes a surface into right triangles and applying a finite difference expression for the total area [22].

Courant developed, in 1943, the method as it is known in current days, without reference to Schellbach's work. Only in the 1950s engineers in aeronautical field made progress by the use of the method in design and structural analysis. During this period the key contributors of the method were Professors Jon Turner, John Argyris and Ray Clough. In 1960, Clough coined the term "finite element", and since then the method has spread to all fields of engineering [1], [22]–[24].

A history tree of finite element method evolution until current days is demonstrated in Figure 2-1, which shows the contribution of each author from different study fields.

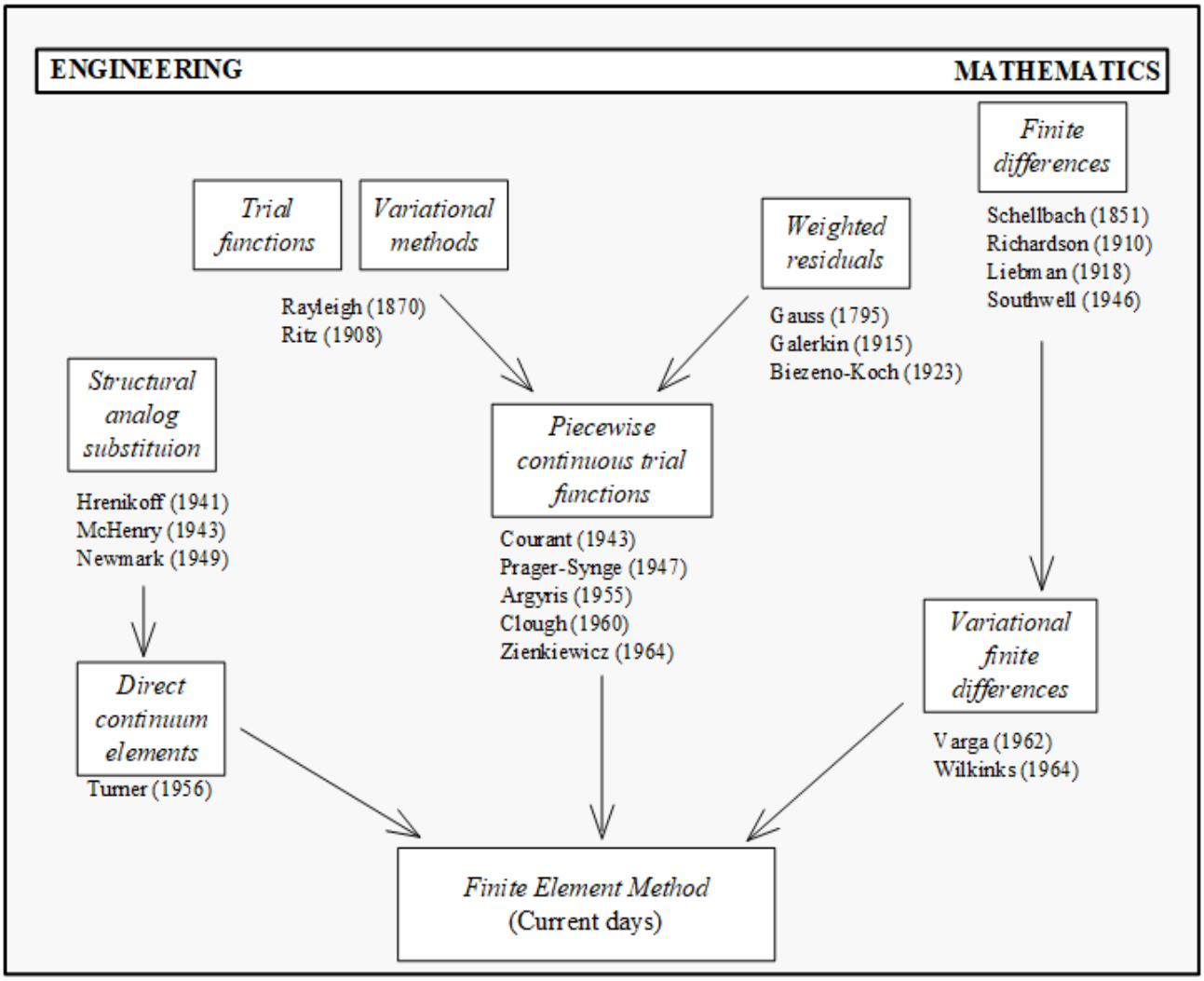

Figure 2-1. History tree. Adapted from [24]**.**

2.3 The finite element method applied to transformers analyses

The use of the finite element method to analyze electromagnetic fields was only possible after several improvements of computational technology, which allowed the studies of electrical machines through this methodology only in the beginning of the 1970's.

In the early days of transformers modeling by the FE method, 1970, Silvester and Chari proposed an analysis of finite element solutions to saturable magnetic fields considering nonlinear magnetics. The technique was classified as a new methodology with one of the initial numerical experiments using the analysis of field problems by the FE method [5].

Through analyses from the software Ansoft, in 1993 Lu and Liu proposed, an analysis by the FE method of DC saturation to verify the susceptibility of transformers to

geomagnetically induced currents. The study includes simulations of single-phase and three-phase transformers, with all the core configuration. The only concern about the simulations results, demonstrated by R. A. Walling, is about the limitation of analyses only to DC excitation, which could present invalid outputs considering real conditions of excitation AC and geomagnetically induced currents excitation [25].

Considering the possibility to solve problems using the FE method in transient domain by external circuits, S. Liu, Z. Liu and Mohammed formulated, in 2007, an analysis of a single-phase distribution transformer working with winding short circuit faults. The results considered outputs not only of a FE tool, but also simulations by Matlab®/Simulink software [26].

In 2017, with the possibility of editing the characteristics of the material, Adame, Kefalas, Martínez and Rojas studied the prediction of core loss considering lamination core steps of single-phase distribution transformers, and compared the performance of M-5 steel and 23ZDKH90 steel at 50Hz, and rated operation conditions [27].

Özüpak and Mamiş, in 2019, modeled a three-phase transformer with the purpose to analyze the relation between electromagnetic flux distribution and thermal behavior. The results compare the two models approach and verify relative errors of an analytical and numerical output.

Chapter 3

3 Review of electromagnetics and power losses

3.1 Maxwell's Equations

The study of electromagnetic phenomena has been developed since the beginning of 19th century, by formulations proposed by scientists like, Gauss, Ampère, Faraday, Lenz and others. But only in 1862, when Maxwell added an extra term to the Ampère law, which allowed a description in a complete way through the interaction between matter and electromagnetic field, and its behavior according fundamental equations (Eq. 3.1 – 3.4) which governing all macroscopic electromagnetic phenomena [2], [8], [14], [20], [28]–[32].

$$\nabla \times \boldsymbol{H} = \boldsymbol{J} + \frac{\partial \boldsymbol{D}}{\partial t} \quad \text{(Maxwell-Ampère law)} \tag{3.1}$$

$$\nabla \times \boldsymbol{E} = -\frac{\partial \boldsymbol{B}}{\partial t} \quad \text{(Faraday's law)} \tag{3.2}$$

$$\nabla \cdot \boldsymbol{D} = \rho \quad \text{(Gauss' law)} \tag{3.3}$$

$$\nabla \cdot \boldsymbol{B} = 0 \quad \text{(Gauss' law – magnetic)} \tag{3.4}$$

The differential form of Maxwell-Ampère law described by the Equation (3.1) has the static portion composed by the original law stablished by Ampère in 1820, also represented for the following equation:

$$\oint \boldsymbol{H} \cdot \boldsymbol{dl} = I \tag{3.5}$$

which states that the integral line of a magnetic field, $\boldsymbol{H}$, in any closed path, $\boldsymbol{dl}$, is equal to current enclosed by that path [8]. This expression is the basic theory to analytical project proposed in Chapter 4, using a magnetostatic approach.

Furthermore, the time variation portion of the Equation (3.1) added by Maxwell represents the displacement current effect, which produces a time-varying, not steady, magnetic field as effective flow of electrical charges, as proposed in the Equation (3.6) also, named of electric continuity [2], [8]

$$\nabla \cdot \boldsymbol{J} = -\frac{\partial \rho}{\partial t} \tag{3.6}$$

where $\boldsymbol{J}$ is the current density and ρ is volume charge density.

As $\boldsymbol{B}$ represents the magnetic flux density, related to magnetic field intensity, $\boldsymbol{D}$ is electric flux density, related to electric field intensity, $\boldsymbol{E}$.

3.1.1 Constitutive relations

Only three of fundamental equations are independent, since the Equations (3.1) and (3.2) combine to Gauss law, Equation (3.3) or (3.4), or with the electric continuity (3.6) building an independent system. In this context, the constitutive relations make Maxwell's equations explicit, considering that they describe the macroscopic properties of the media considered [2], [8], [20] as follows

$$\boldsymbol{D} = \varepsilon_0 \boldsymbol{E} + \boldsymbol{P} \tag{3.7}$$

$$\boldsymbol{B} = \mu_0 (\boldsymbol{H} + \boldsymbol{M}) \tag{3.8}$$

$$\boldsymbol{J} = \sigma \boldsymbol{E} \tag{3.9}$$

being $\boldsymbol{P}$ the polarization vector, $\boldsymbol{M}$ the magnetization vector, the constants in the vacuum, ε_0 and μ_0, are respectively, electrical permittivity, magnetic permeability and σ is the material conductivity.

For linear materials the polarization and magnetization are directly proportional to the electric and magnetic fields, as described in Equations (3.10) and (3.11)

$$\boldsymbol{P} = \varepsilon_0 \chi_e \boldsymbol{E} \tag{3.10}$$

$$\boldsymbol{M} = \chi_m \boldsymbol{H} \tag{3.11}$$

being χ_e the electric susceptivity and χ_m the magnetic susceptivity.

Considering linear media, isotropic and homogeneous, the constitutive relations, (3.7) and (3.8) are reduced to:

$$D = \varepsilon_0(1 + \chi_e)E = \varepsilon_0\varepsilon_r E = \varepsilon E \tag{3.12}$$

$$B = \mu_0(1 + \chi_m)H = \mu_0\mu_r H = \mu H \tag{3.13}$$

where ε_r and μ_r are relative permittivity and permeability, respectively, and ε and μ the absolute permittivity and the permeability of material [2], [8], [20].

3.1.2 Vector magnetic potential field

From the Gauss' law of magnetism, the magnetic flux density, $\boldsymbol{B}$ can be defined by the magnetic potential field vector, $\boldsymbol{A}$, therefore $\boldsymbol{B}$ is solenoidal in the whole space. This relation is demonstrated in Equation (3.14). Furthermore, by consequence of Faraday's law (Eq. 3.2) the electric field is demonstrated as a relation between the magnetic potential field vector and the electric scalar potential, *V*, as shown in Equation (3.15) [2], [3], [8], [20].

$$\boldsymbol{B} = \nabla \times \boldsymbol{A} \tag{3.14}$$

$$\boldsymbol{E} = -\nabla V - \frac{\partial \boldsymbol{A}}{\partial t} \tag{3.15}$$

3.1.3 Electro and magnetostatic fields

In stationary systems there are no time-varying terms, thus, the induced and displacement currents are neglected, resulting in the following Maxwell's equations to static fields.

$$\nabla \times \boldsymbol{H} = \boldsymbol{J} \tag{3.16}$$

$$\nabla \cdot \boldsymbol{B} = 0 \tag{3.17}$$

$$\nabla \times \boldsymbol{E} = 0 \tag{3.18}$$

$$\nabla \cdot \boldsymbol{D} = \rho \tag{3.19}$$

Therefore, by a combination among Equations (3.13), (3.14) and (3.16), the resulting equation used by FE tool, ANSYS/Maxwell®, to formulate the electromagnetic problems in static domains is given by the Equation (3.16) [33], [34].

$$\nabla \times \left(\frac{1}{\mu}\nabla \times \boldsymbol{A}\right) = \boldsymbol{J} \tag{3.20}$$

3.1.4 Time-varying fields

In time-varying field analyses the Equations (3.21) and (3.22), resulted from combination between Gauss's law (Eq. 3.3) and electric field, defined by magnetic potential vector, $\boldsymbol{A}$, (Eq. 3.15), which is used to formulate electromagnetic problems [8].

$$\nabla^2 V - \mu\varepsilon\frac{\partial^2 V}{\partial t^2} = -\frac{\rho}{\varepsilon} \tag{3.21}$$

$$\nabla^2 \boldsymbol{A} - \mu\varepsilon\frac{\partial^2 \boldsymbol{A}}{\partial t^2} = -\mu\boldsymbol{J} \tag{3.22}$$

It is important to highlight the use of the identity (Eq. 3.23) and the condition (Eq. 3.24)

$$\nabla \times \nabla \times \boldsymbol{A} = \nabla(\nabla \cdot \boldsymbol{A}) - \nabla^2 \boldsymbol{A} \tag{3.23}$$

$$\nabla \cdot \boldsymbol{A} = -\mu\varepsilon\frac{\partial V}{\partial t} \tag{3.24}$$

3.2 Losses' review

3.2.1 Core loss

The material used in the transformer's core is a soft magnetic iron, with high permeability. The application requires material easy to magnetize, by a low magnetic field [14]. Predict iron loss is a hard task as it involves microscopic phenomena, whereas the forecasting uses parameters in a macroscopic scale, as magnetic flux density and magnetic properties [20], [35].

An indicator used to monitor the quality of the soft ferromagnetic material is a low magnetic loss. The classic model of prediction of magnetic losses is defined by the sum of the loss portion relating to hysteresis loss and the component due to induced eddy-currents.

Hysteresis loss represents the power required to magnetize the material and that is not recovered completely when the applied magnetic field is decreased till zero, which is translated by the area of the hysteresis loop (Figure 1-2). The eddy-current loss is a result of induced current into the core's material due to the variable magnetic flux across it, also called Foucault's currents [6], [14], [20], [36]–[38].

The forecasting model used to predict core loss is useful in a qualitative analysis of electric devices, however, does not offer a high accuracy of losses in ferromagnetic materials of the electric machines' core.

The iron magnetization happens in time and space domain, according to material structure and orientation of domains, and even in slow variation of magnetic fields there exist fast magnetization variations, which are not included in the classic model [20]. The loss portion related to excessive losses can be described traditionally as microscopic eddy-currents induced on domain wall movement locally in the lamination. The core's lamination is a method to reduce the induction of eddy-currents and consequently reduce the losses [20], [39], [40].

As a result of combination among the classical portion of core loss, hysteresis and eddy-current, and the excessive losses' portion, the expression that describes the iron loss model for maximum magnetic flux density (B_m) and frequency (f), where the skin effect is negligible, is shown on Eq. (3.25)

$$p_{cr} = k_c(fB_m)^2 + k_h f(B_m)^{\beta} + k_e(fB_m)^{1.5} \tag{3.25}$$

where k_c is eddy-current coefficient and is given by Eq. (3.26)

$$k_c = \pi^2 \sigma \frac{d^2}{6} \tag{3.26}$$

being σ the conductivity of material and d the thickness of lamination sheets. The coefficients associated to hysteresis loss k_h and β are estimated by the adjustment of experimental hysteresis loss curves, associated for a range of magnetic flux density and frequencies. For simplification purposes, the term β is assumed as 2, then the FE tool chosen uses that approximation. The coefficient associated to excess loss is also calculated with results from experimental tests for a specific frequency and magnetic flux density. It is important to highlight that the only component of these losses possible to estimate without experimental results is the eddy-current loss [20], [33], [40].

For non-sinusoidal field excitation, the exemplified model is not efficient, being necessary Fourier series expansion of magnetic flux density. Deng (1999) proposes a

modification of iron loss model to include harmonic parameters of flux density, using a correction factor to compute hysteresis cycles with smaller amplitude than B_m. However, even the proposed modification improves the iron loss forecast, it still depends of experimental tests [20], [40].

3.2.2 Resistive loss

The greatest portion of power losses in an electric machine is characterized by the Joule power loss, also called resistive loss or ohmic loss, responsible for the windings' heating [20]. Considering the wire diameter less than the skin depth at industrial frequency, the AC component of resistive loss is neglected, and the DC resistive loss of one winding, related to transformer material winding resistance, *R*, and the associated current *I*, is given by:

$$P_J = RI^2 \tag{3.27}$$

In case of the current density known in each point of the structure in a planar symmetry (*xy*), the instantaneous resistive loss is determined by the integral [3]:

$$P_J(t) = \int \rho {J_z}^2 dS \tag{3.28}$$

where ρ represents the electric resistivity of the conductor at a given temperature of the winding and J_z is the current density in direction of *z* axis.

3.2.3 Stray losses

The stray losses may contribute to the degradation of the machine's performance, since it contributes to an extra temperature rise. Understanding the phenomena that cause this portion of losses is essential to evaluate the design's efficiency of the machine under study [37].

In the initial stage of modeling an electrical machine, only the portion of losses associated with the fundamental frequency of field is assumed. However, since the stray losses caused by the magnetic leakage and fringing flux and their harmonics, in additional to the fundamental losses, is necessary regarding another portion of Joule loss and core loss associated to harmonics [37], [41].

Traditional methods to estimate these loss components have a high degree of uncertainty, thus, experimental procedures are usually used to predict this portion of losses. The

loss components related to core losses and stray load losses are associated to open circuit and short circuit tests, respectively [41].

In the absence of an effective analytical model to predict stray losses, the estimation of these losses is accomplished based on a percentage of the power supplied by the machine (P_s), Equation (3.29) [20], [42].

$$P_{str} = k_{str} P_s \tag{3.29}$$

The standard IEC determine the percentages of input power, in induction machines, which represent the stray losses based on the function shown in Figure 3-1 [42].

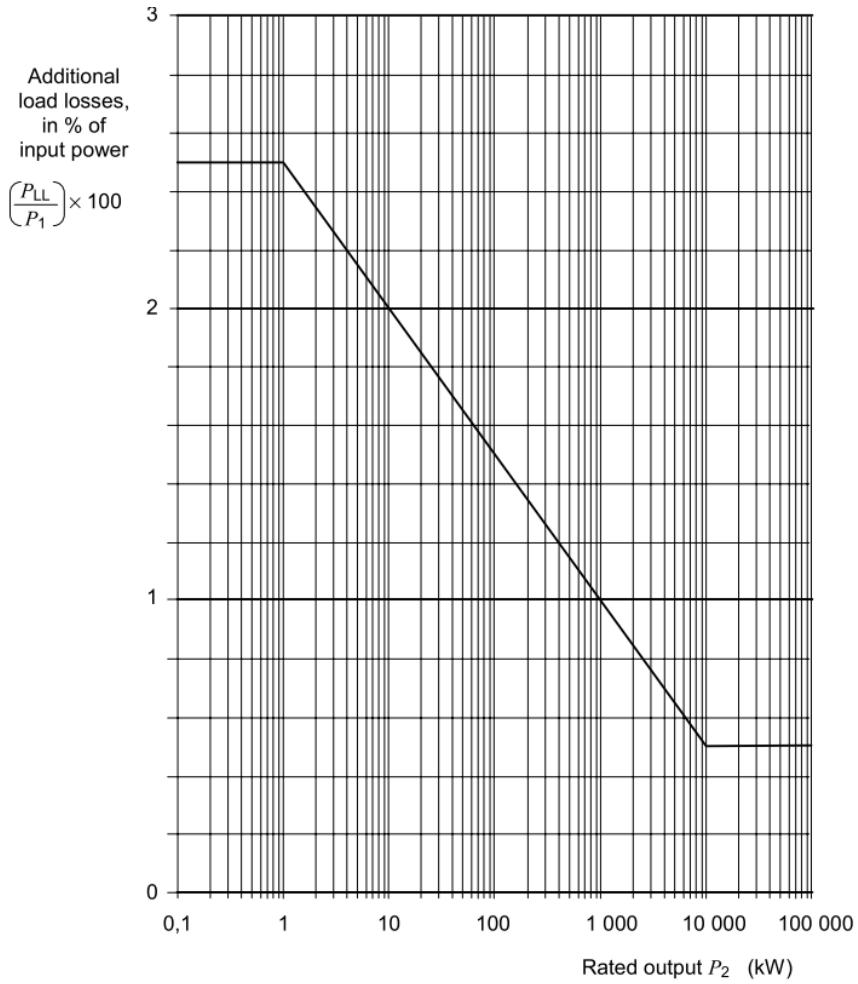

Figure 3-1. Stray loss curve [42].

For low power machines, with output power lower than 1kW, it is stablished that the portion of stray losses is 2.5% of the power supplied. However, this parameter has a medium-high uncertainty, therefore, to stray loss parameter has a high accuracy are necessary experimental testes [20].

Chapter 4

4 Analytical electromagnetic design approach

The analytical approach of the electromagnetic design allows the analysis of the magnetic flux density in the ferromagnetic material, which composes the transformer's core, and evaluates if the machine is operating in saturation conditions. The analysis consists of duality between the electrical circuit principle and the magnetic circuit, called reluctance network.

Ampère's law (Eq. 3.5) is the main principle of magnetic circuit analysis, with the additional parameter of the number of turns, *N*, in each winding, as demonstrated in Equation (4.1)

$$H = \frac{NI}{l} \tag{4.1}$$

where *l* is the length of magnetic flux middle path.

In magnetic circuit analysis the magnetomotive force $\mathscr{F}$, product of multiplication of the number of turns and the associated current (Eq. 4.2) is the dual of electromotive force. On the other hand, the magnetic flux, Φ, has a behavior that can be modeled as an electric current. In this last comparation has an error source of this duality, since the electric current flows in the close path given by the conductor, the magnetic flux can flow out of the magnetic circuit, being this phenomenon known as leakage flux.

Thus, the problem is formulated by Equation (4.3), and considered the established relations given by Equations (4,1), (3.13), (4.2), consecutively.

$$\mathscr{F} = NI \tag{4.2}$$

$$\mathscr{F} = \mathscr{R}\Phi \tag{4.3}$$

The reluctance, $\mathscr{R}$, is a measure of the opposition to the flux offered by the magnetic circuit [43]. This magnitude involves the core's dimensions, specifically the sectional area, A_s,

and the length, l. The obtained equation is similar to the resistance of an electric wire, as shown by the followed equation.

$$\mathscr{R} = \frac{l}{\mu \cdot A_s} \tag{4.4}$$

Considering that the absolute magnetic permeability, μ, product of relative permeability and the permeability in the vacuum, varies along the magnetization curve, which has a nonlinear behavior, the iron characteristics are introduced in the calculation of reluctance network by an iterative process, shown in Figure 4-1. The stopping criterion defined in the reluctance iterative calculation is the absolute error, $|\mathscr{R}^{i} - \mathscr{R}^{i-1}|<10^{3}$.

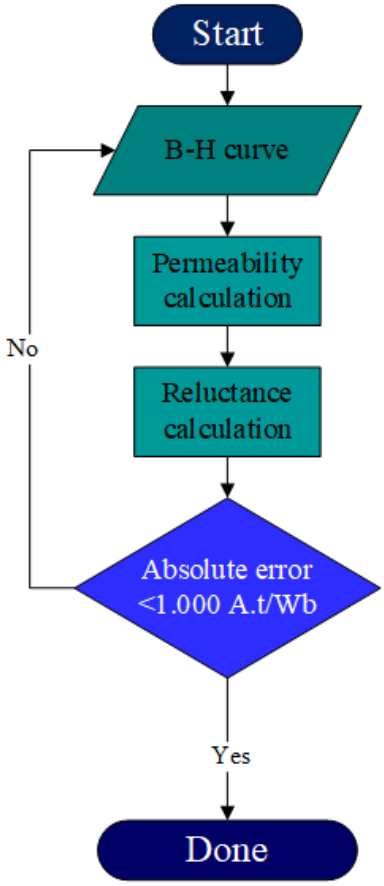

Figure 4-1. Iterative process

The relative permeability, μ_r, is estimated from magnetization curve (Figure 4-2), i.e., the ***H-B*** curve, and Equation (3.13), of which the value of magnetic permeability in the vacuum, μ_0, is $4\pi \times 10^{-7}$ H/m. For the magnetic characteristics of ferromagnetic material under study, and considering the stopping criterion for the iterative calculation, the relative permeability considered in the analytical project is 2017.

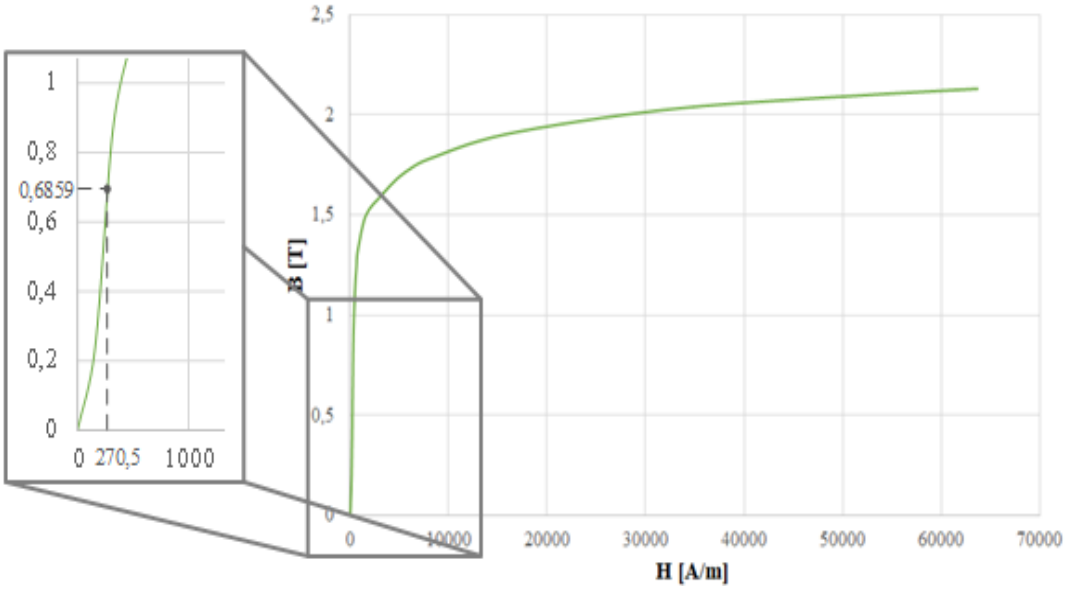

Figure 4-2. Zoom on magnetization curve. Adapted from [18].

The final reluctance network (Figure 4-3) with two feed sources representing the magnetomotive forces modeling excitations of the high voltage winding, $\mathcal{F}_{HV}$, and low voltage winding, $\mathcal{F}_{LV}$. Those sources are represented by opposite polarities, considering the arrangement of windings' turns.

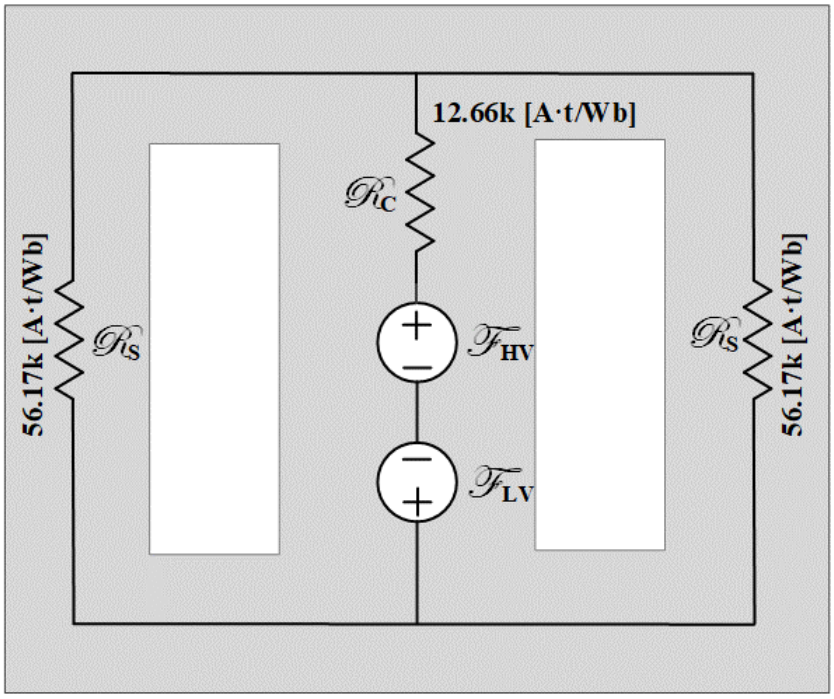

Figure 4-3. Reluctance network.

The reluctance network allows essentially to verify if the core's material is saturated, which implies a in a higher reluctance path, and requires the increase of the magnetomotive force to keep the same magnetic flux on the system [25]. But even the reluctance network allowing

analyzes the magnetic flux density in points around all the core surface, the low number of elements modeled by the reluctances network, does not allow a high degree of discretization as the FE method allows, presented in Chapter 5.

Chapter 5

5 The finite element method design approach

The Finite Element Method (FEM) consists of a numerical solution based in partial differential equations (PDE) to solve mathematical problems in a complex domain, with associated boundary conditions [1], [2], [20].

The definition of the finite element can be described as a division of domain into finite number of smaller subdomains, where the PDE are applied to each of them. In electromagnetic analysis, these numerical methods use the solutions of Maxwell's equations to determine the distribution of the electric and magnetic fields [3]. The model proposed by this work use as FE tool the commercial software ANSYS®, Maxwell package.

5.1 Two dimensional versus three dimensional analyses

A 3D analysis is usually suggested to study electromagnetic fields distribution. However, this approach requires to model the whole structure, which means a heavy processing and consequently a long computation time. That way, an advantage of the 2D approach is the decrease of the number of elements resulting in faster simulations [3], [20].

Another advantage related to a bidimensional analysis is the possibility to explore symmetries around all the complex domain, being necessary just the set of boundary conditions of the area under analysis. In this context, is assumes that the field distribution around the model has no variation in the third dimension, which allow an easier output interpretation.

The device discussed is shown in 3D model in Figure 5-1 (a), and Figure 5-1 (b), representing the front cutting edge of the transformer. The area presented in Figure 5-1 (b) assumes the magnetic potential vector as the same through *z* axis.

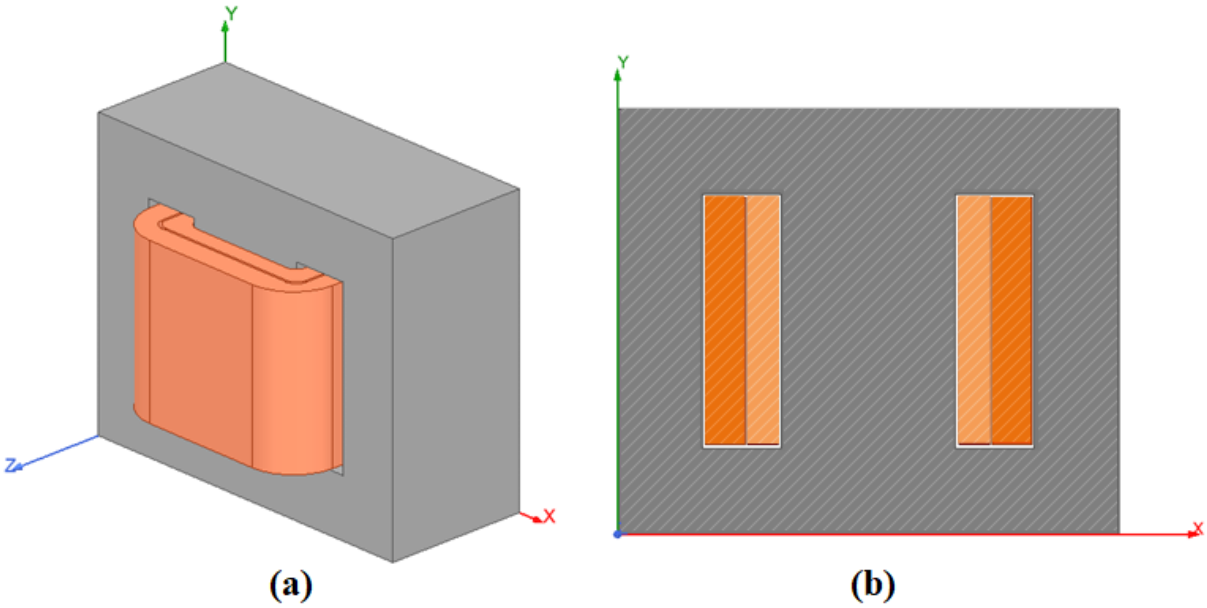

Figure 5-1. (a) 3D model; (b) 2D model.

5.2 Solution type

The two solver approaches chosen to validate the model of transformer under analysis are related to magnetic magnitudes, *eddy-current solver* (magnetostatic domain) and *magnetic transient solver*. The solver options provide by the ANSYS®/Maxwell is shown by Figure 5-2.

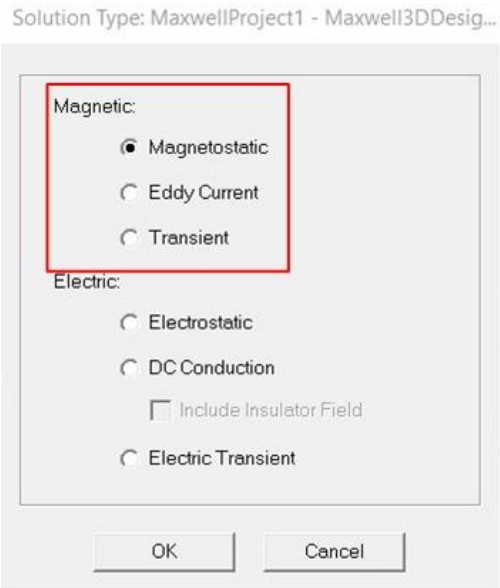

Figure 5-2. Solution type

5.2.1 Eddy-current solver

The *eddy-current* solver computes the problem considering steady-state operation at a given frequency and assumes that frequency as the pulsating fields through the domain. The 3D approach is a full wave solver and also considers in the calculation displacements currents. To perform the domain discretization, the *eddy-current* solver consider an adaptive mesh technique to get the best mesh required by the accuracy level required [33].

This approach allows detailed sets of losses by equations described in section 3.2, and the algorithm that describes the solution process of *eddy-current* solver is shown in Figure 5-3.

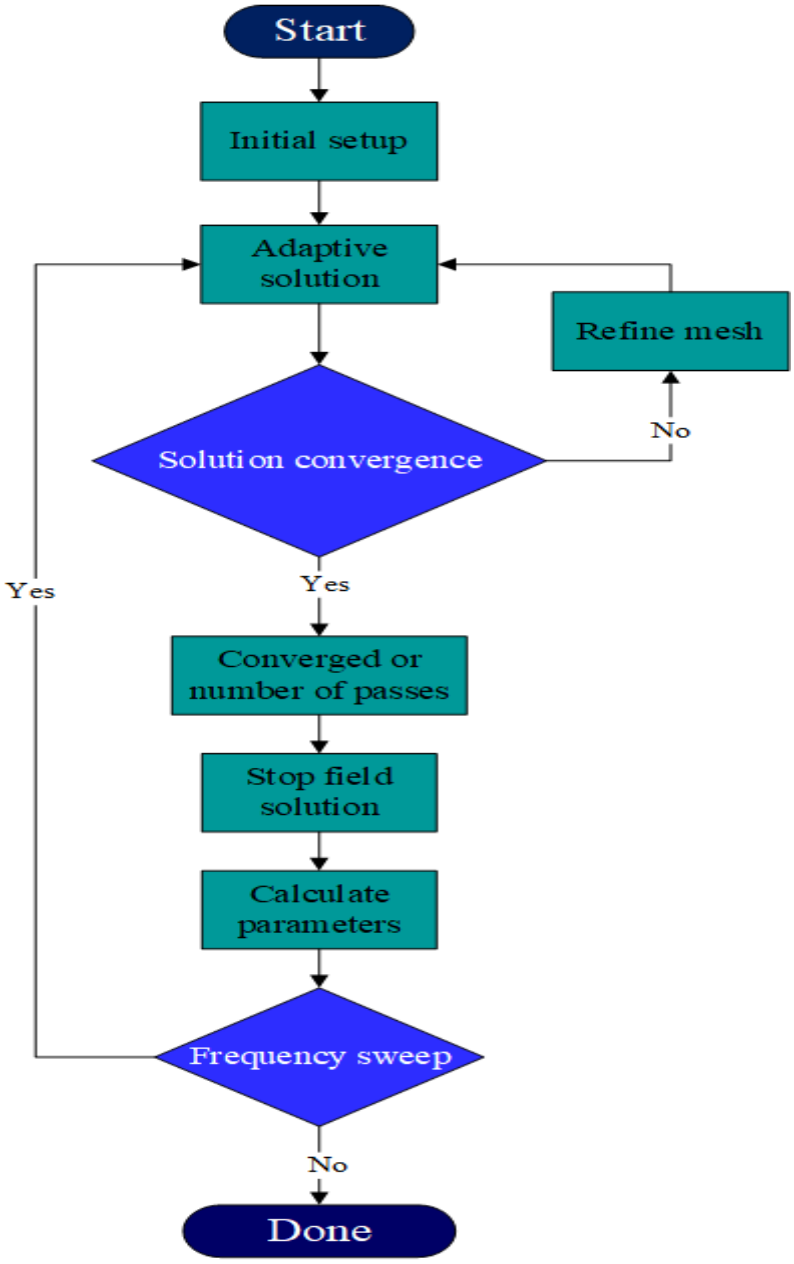

Figure 5-3. *Eddy-current* solver diagram. Adapted from [33]**.**

5.2.2 Magnetic transient solver

The *magnetic transient* solver computes time-varying magnetic fields, in a time domain solver or for instantaneous magnetic fields. The source used in a simulation can be modeled by regular voltage/current excitation, sinusoidal sources (external circuit) or varying permanent magnets. Hence, this solution type does not use adaptive mesh refinement, being necessary to create and refine the mesh using mesh operations or a linked mesh to obtain the necessary accurate mesh [44].

As a result, the diagram presented in Figure 5-4 demonstrates the algorithm of solution process of *magnetic transient* solver.

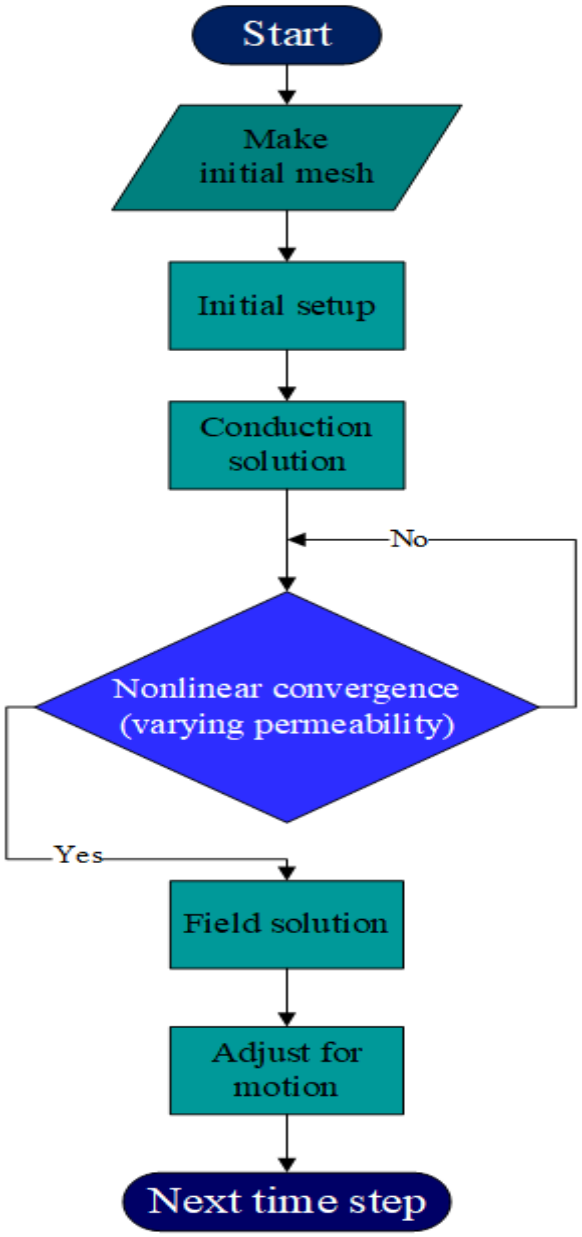

Figure 5-4. *Magnetic transient* solver diagram. Adapted from [44]**.**

5.3 Boundary conditions

The explanation of boundary conditions considering a planar symmetry to simplify the visualization of field problems. Therefore, the involved currents, in the transformer under study, are perpendicular with the model plane, consequently the magnetic field has only components in the plane ***xy***. As a result, the magnetic potential vector is in positive direction of axis *z*, so its only component is A_z [3], [20].

Accordingly, the selection of boundary conditions is fundamental in the solution of field problem, because these conditions not only influence the final result, but also the reduction of domain under analysis, which influences the simulation time.

5.3.1 Dirichlet's condition

In this condition the magnetic flux lines are tangential to the boundary, without crossing it. Usually, the homogeneous Dirichlet's condition, that set the A_z as zero, is used to external boundary of the electrical machine. Consequently, it is equivalent to considering the external space of the object magnetic isolating, with a null permeability [3], [20].

The software ANSYS®/Maxwell 2D, applies this condition with boundary type *Magnetic vector potential*, where is necessary to configure the parameter as zero. In a 3D approach the condition is considered in the boundary type *Insulating* [21], [45].

5.3.2 Neumann's condition

Neumann's condition is used to modeling an incidence angle of magnetic flux lines at the boundary. The homogeneous conditions force the flux lines to be perpendicular to the boundary. Consequently, in magnetic analyses, the magnetic flux density vector (*B*) has only a normal component related to the boundary line [3].

In terms of the software, the boundary type used to set this condition is named after itself, as *Neumann* [21], [45].

5.3.3 Periodic condition

The periodic condition is useful in problems that requires to emulate the symmetry of design, by periodic behaviors of magnetic vector potential around two or more boundaries of the structure. Those repetition is divided in two categories, odd or even periodicity [3], [20].

This condition is set on the software by the boundary type of *Symmetry*, to 2D and 3D analysis approach [21], [46].

5.4 Partition of the domain

The discretization of domain is the stage in which the model is defined by a great number of small elements. Those elements define the accuracy of the solution, according to the dimension and the adaptive capacity to the model, in order to have a better resolution of fields distribution.

Each problem requires a type of mesh. In 2D, in which the domain is a surface and the subdomains are a polygonal, normally triangular or rectangular elements are used(Figure 5-5 (b)). In case of 3D model, the domain is a volume and each subdomain is a triangular prism, rectangular solid or tetrahedron (Figure 5-5 (c)). For complex geometries, the triangular or tetrahedron element has better efficiency due to its capacity to adapt to corners, curves and boundaries [2], [3].

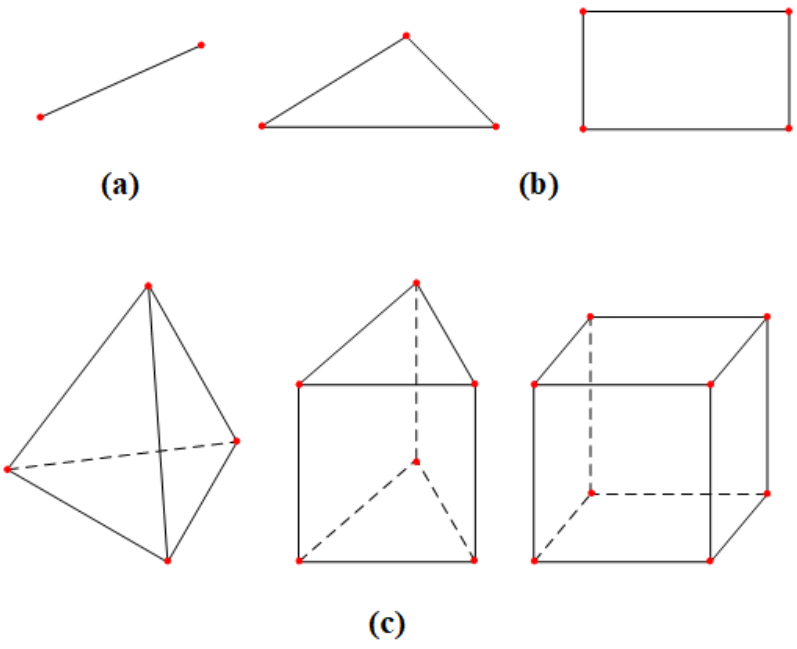

Figure 5-5. Elements for the partition of the domain. (a) 1D; (b) 2D; (c) 3D. Adapted from [2].

The software ANSYS/Maxwell®, for statics solvers uses the automatic creation of mesh on all solids, before the solving procedure. Therefore, the process consists of using the initial mesh to run the field calculation. The adaptative mesh is a tool to refine the initial mesh and improve the field distribution in areas that need a better resolution, like for example, corners and holes. As a result, the mesh quality is based on the energy error report, that evaluates the mesh refinement ability in each pass of the calculation process [47].

5.5 Postprocessing

The postprocessing is the stage when it is possible to analyze the results of the model under analysis. In this final step, the outputs are not only related to the fields problem, but also it make possible verify the solution data, that verify the convergency, mesh statistics and quality, report plots, which are very useful in transient analyses, and fields calculator [19].

The output parameters used to evaluate the results during all simulations are discretized in the following sections.

5.5.1 Solution data

The solution data provides information about the solution process, and it also can be checked during all the process. In addition, it contains information about the software performance, simulation time and the physical memory used for each task.

Regarding the convergence information, the mesh analysis is given by the number of elements used to discretize the domain and the percentage energy error, which measures the quality.

In case of losses analyses, the solution data provides the results of each type of loss considering the whole volume analyzed.

5.5.2 Field Overlays

The main output required to the finite element method tools is the field overlays. Those results with high degree of discretization is the main advantage of the method.

The field plots can be a contour or vector plot and the results can be of basic magnitudes, like magnetic flux density, magnetic field, current density and electric field, or even derived

magnitudes, such as resistive and core loss [19]. Furthermore, the field creates tool that allow plotting the field distribution through the object or only on the surface.

5.5.3 Report plots

The tool of rectangular report plots is useful to analyze graphics of time-varying parameters. In case of electrical machines, those reports allow to verify the currents and voltages behavior, according to the excitation of the windings.

Another possibility from this tool is tracing characteristics to add computational functions to the trace data and improving the plots results.

Chapter 6

6 Results and discussions

6.1 Experimental results

Experimental tests were implemented in order to verify the core and resistive losses in a physical prototype under rated excitation conditions. All the electrical and physical parameters used in the simulations match with real parameters. However, the real core material is not known being assumed the same magnetization (Figure 1-3) and B-P curve (Figure 1-4) as used by the finite element tool. The physical prototype used to experimental texts is shown in Figure 6-1.

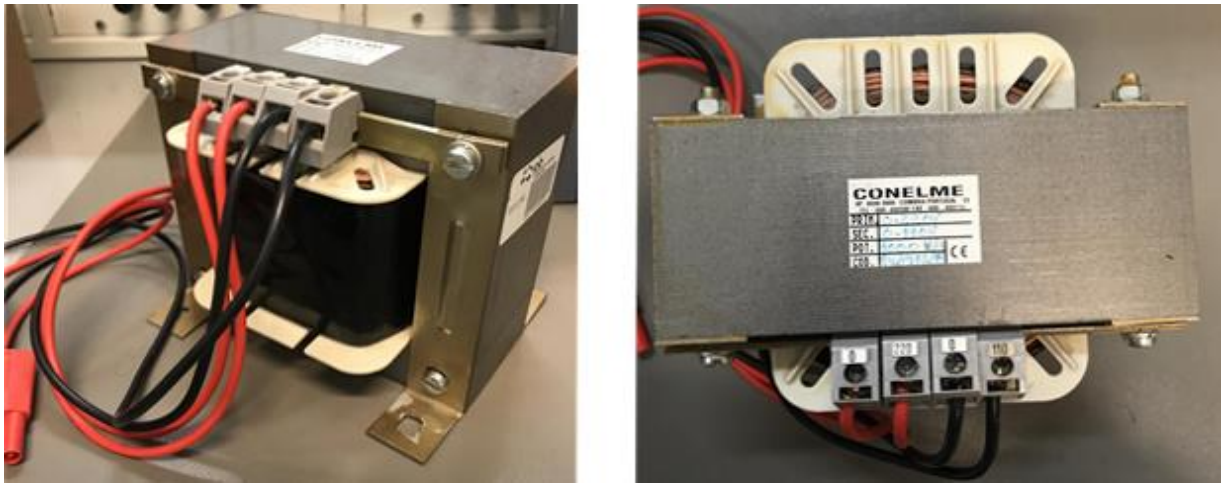

Figure 6-1. Physical prototype

The power losses measured in experimental test are presented in Table 6-1, where core loss was obtained from no-load test and the resistive loss is the result of a short-circuit test. The experimental tests occurred at room temperatures and flowed of each other, in a short period of time.

Also, the no-load test allowed the determination of the real transformation ratio of the transformer, given by voltage 220/116V_{rms}, considered in the FE simulations, redefining the number of turns of HV winding proposed in Appendix A.

Table 6-1. Experimental power losses

	Losses (W)
No-load	13.00
Short circuit	41.00

6.2 Finite element outputs

6.2.1 Mesh quality

The software ANSYS®/Maxwell, for statics solvers, uses the automatically creation of mesh in all solids before the beginning of the solution process. The process consists of the use of the initial mesh to perform the field calculation and refine this mesh, in order to improve the field distribution around the structure [47].

In conclusion, the mesh quality is based on the energy error reported, which evaluates the mesh refinement capability in each step of calculation process [47]. In Figure 6-2 it is possible to observe the energy error decrease according to the number of elements. This test was made in magnetostatic domain by the 2D approach, besides the limitation of maximum number of passes in ten iterations.

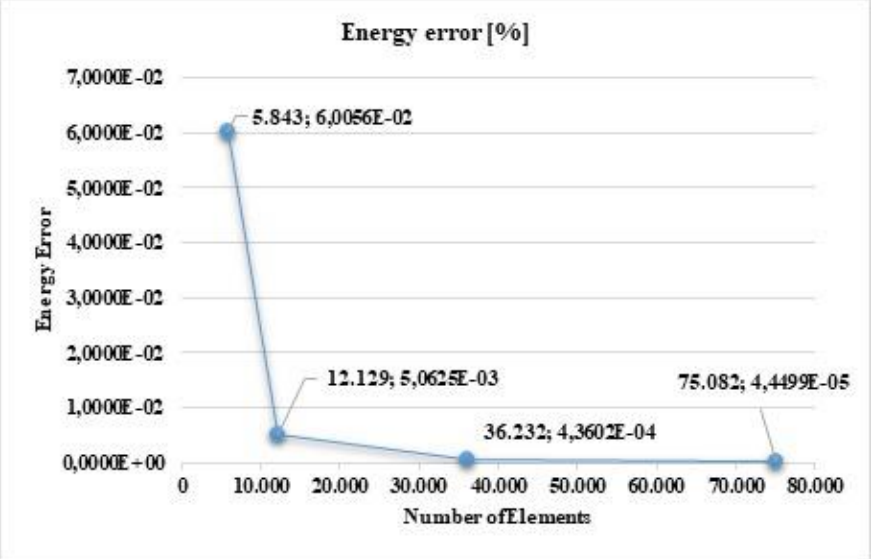

Figure 6-2. Graphic of percentage energy error

For the mesh refinement were stipulated some convergence standards. After several tests, the final model consists in a refinement per pass of 20%, and the adaptive setup specified a percentage error of 0.001%, with a restriction to the element length of 5 mm. The final mesh for the described setup is shown in Figure 6-3 (a).

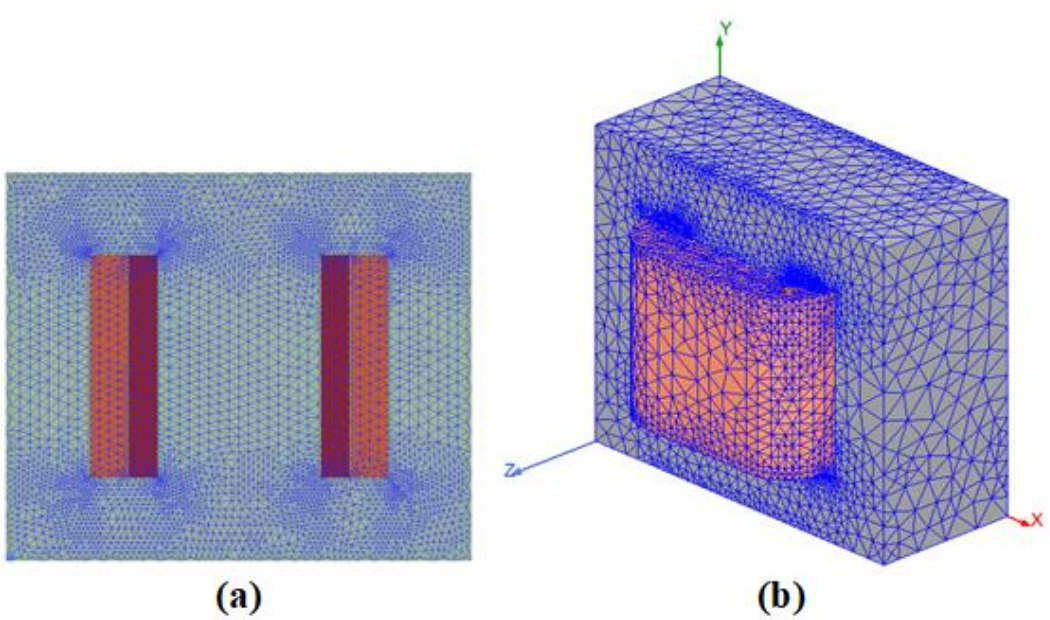

Figure 6-3. (a) 2D Figure 6-3mesh, 75,082 elements; (b) 3D mesh, 284,523 elements.

The mesh quality is presented by a range between [0,1] of percentage error, and the output of the model was 4.45×10^{-5}%. Another output to analyze the mesh quality is the standard deviation (Std) of area, which resulted in the maximum value of 1.72×10^{-6} mm^2. The low values of percentage error and standard deviation support the final mesh quality.

All the standards used in the adaptive mesh of the 2D approach were not able to be applied in the 3D simulations, because the discretization around the whole volume requires a huge computation memory. Thus, the final mesh used in the 3D analyses is shown in Figure 6-3 (b).

6.2.2 Magnetic flux density

The analysis of the magnetic flux density distribution in elements of electric machines allow to verify the point through which the devices are working in saturation conditions. Thereby, even the reluctance network allows to predict the behavior of the magnetic flux density around different points of the machine geometry, does not have an accuracy similar to the FE analysis, because of the low density of elements modeling the network.

A 2D approach was selected to analyze the magnetic flux density distribution, considering that the analytical project of reluctance network was also developed based in a 2D approach. Figure 6-4 presents the distribution of the magnetic flux density around the single-phase E-core transformer under no-load and rated conditions, respectively. It is important to highlight that a 2D analysis considerers the behavior of the flux repetitive for all *z* axis.

Moreover, the results from the reluctance, given by the magnetic flux density (***B***) according to the reluctance of each column of the transformer's core, are overlapped in the Figure 6-4, for comparative purposes.

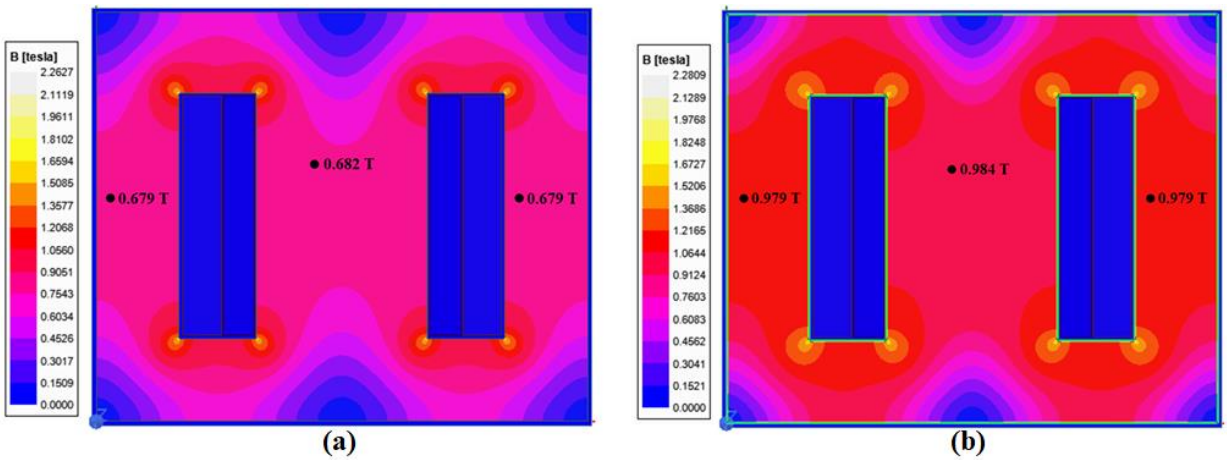

Figure 6-4. (a) No-load test; (b) Rated current test.

The vector flux distribution, at the rated transformers conditions and illustrated in Figure 6-5, expresses the behavior of magnetic flux in the boundaries, according to the set in the previous configurations. In that case, the transformer's external area is magnetically insolated by the Dirichlet's condition, set as $A_z = 0$, in the boundary.

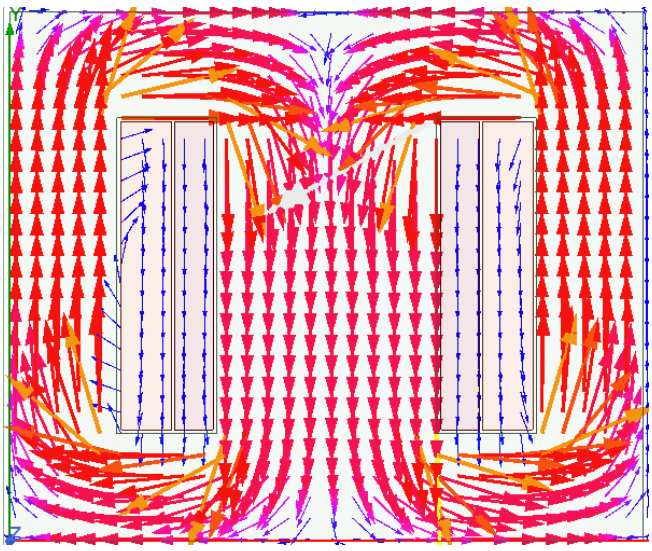

Figure 6-5. Flux distribution in a plane domain

The comparative results of the magnetic flux density analyses, from the analytical project and finite element approach, are presented in Table 6-2.

Table 6-2. Comparative outputs, B.

	Flux density (T) (Analytical analysis)	Flux density (T) (FE analysis)	Relative error
No-load operation	0.679	0.829	22.09 %
Rated operation	0.979	1.140	16.44 %

As expected, the relative errors obtained by the comparison of two approaches come from the divergence of the discretization levels between the analytical and finite element methodologies. It should be mentioned that, both methodologies consider the variation of magnetic permeability as defined by the B-H curve. Although the relative errors are considerably higher, the flux behavior and the calculated parameters are consistent by comparing the two methods.

6.2.3 Electric magnitudes

The *magnetic transient* solver was used to verify the relation between applied voltages of windings and the resulting currents from this excitation. The voltage excitation chosen to evaluate the electric behavior of induction in model designed, at rated operation conditions, is presented in Figure 6-6, in which the red curve is associated to the high voltage (HV) winding and the blue curve is related to the low voltage (LV) winding.

Similarly, the resulted currents in each coil are shown in Figure 6-7, with the same color code stipulated for the voltages, associated to rated excitation of 220/116V_{rms}.

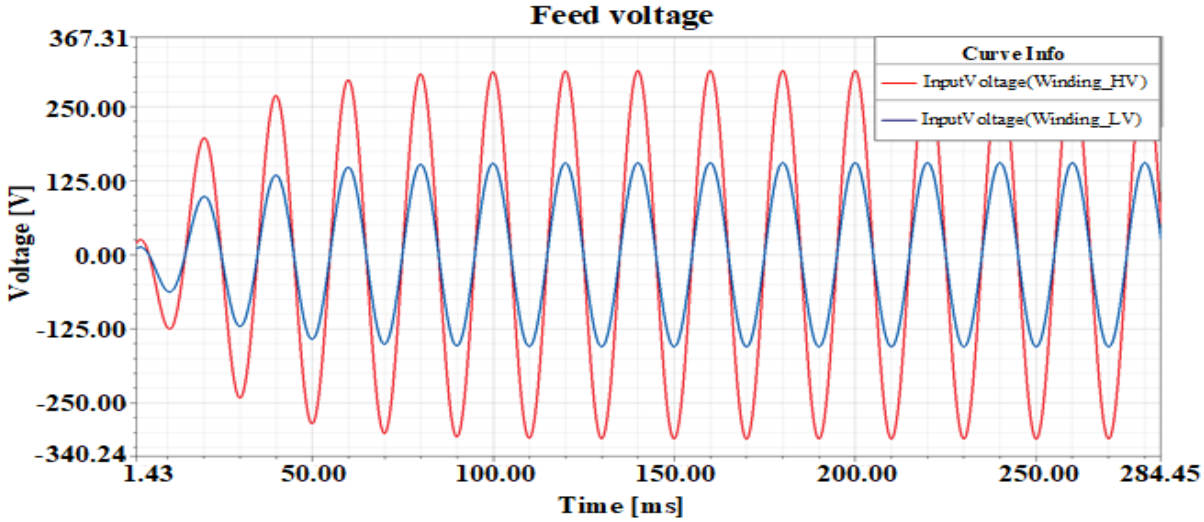

Figure 6-6. Sinusoidal feed voltage

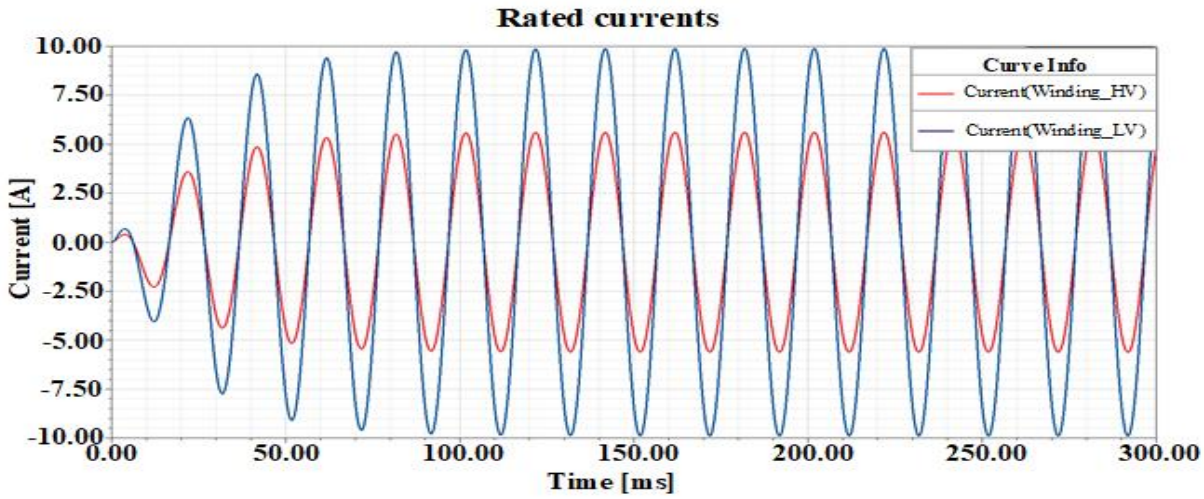

Figure 6-7. Sinusoidal rated current

The flux linkage of high and low voltage windings are shown in Figure 6-8.

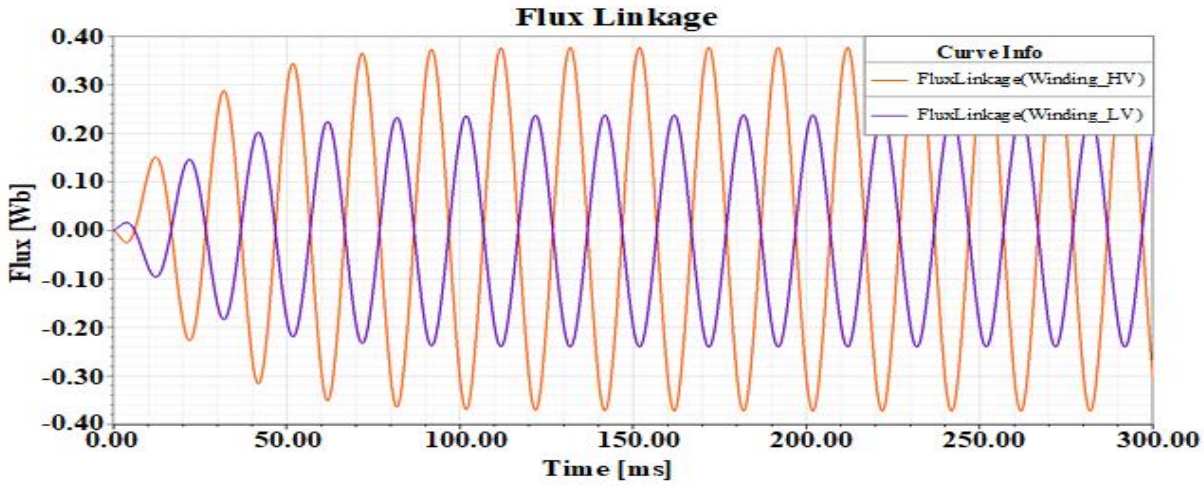

Figure 6-8. Flux linkage.

6.2.4 Core loss

The the estimation of core loss in rated operation by the B-P curve, which has a nonlinear behavior, is used to calculate the loss coefficients at a frequency of 50Hz. The coefficients used to find loss data according to Equation (3.25) and explained in section 3.2.1, are shown in Table 6-3.

Table 6-3. Core loss coefficients

Loss Coefficient	(W/m^3)
K_h	82.225
K_c	0.599
K_e	5.500

Based in this model, the distribution of core loss with rated currents windings excitation is presented in Figure 6-9. Table 6-4 showns the total value of the core loss considering the integral of the whole volume domain, given a satisfactory relative error, when compared with experimental results.

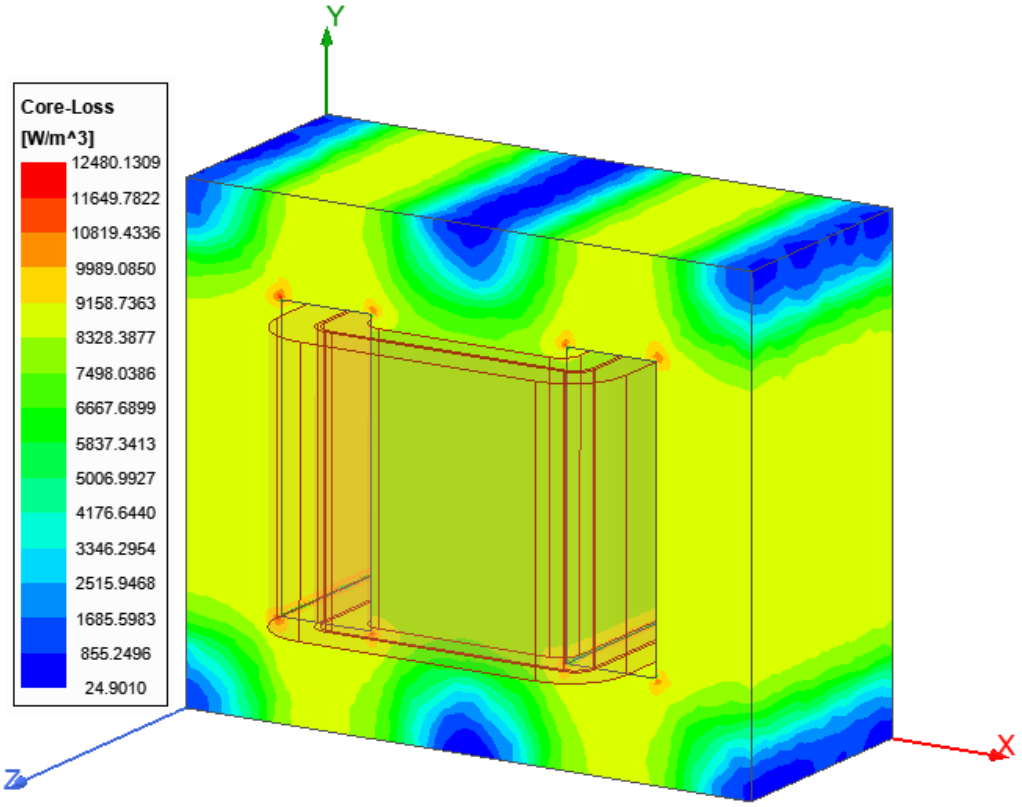

Figure 6-9. Core loss distribution by rated current operation.

Table 6-4. Comparative outputs, core loss.

	Core Loss (W) (Experimental test)	Core Loss (W) (FE analysis)	Relative error
Total core loss	13.00	13.37	2.77 %

6.2.5 Resistive loss

The resistive loss can be calculated using the current density (***J***) at some close volume, as previously introduced by the Equation (3.28). The vector ***J*** distribution, considering steady-state and rated operation is shown in Figure 6-10.

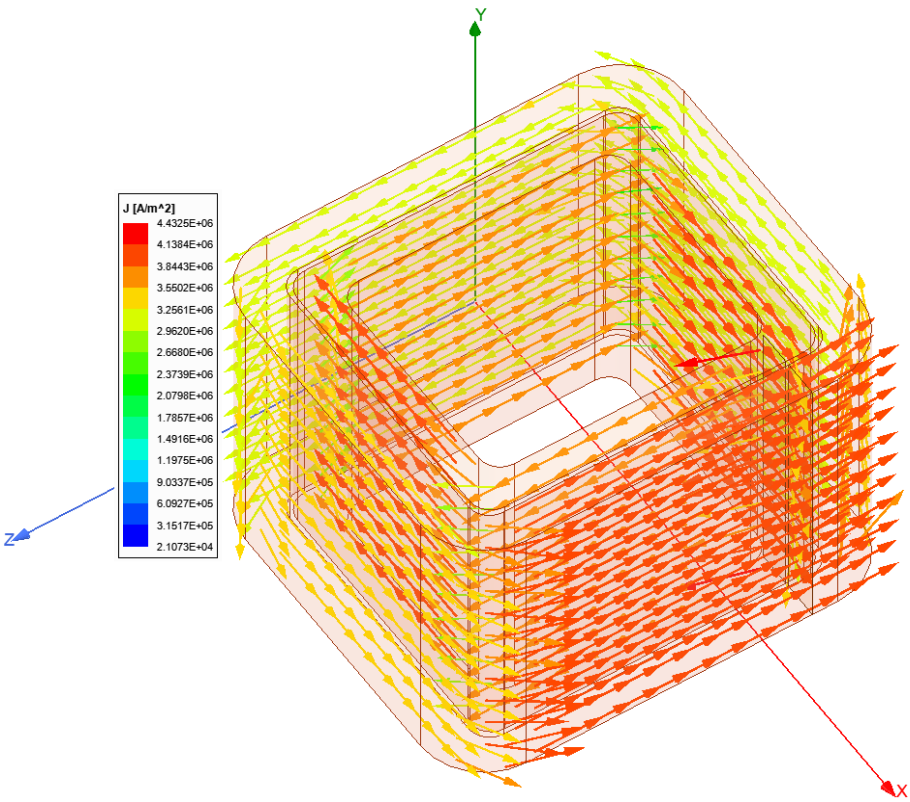

Figure 6-10. Vector current density

The resistive loss distribution from the windings are highlighted by Figure 6-11, according to the current applied in each coil around both windings. The comparative analysis between total resistive loss from the finite element method and experimental tests are found in Table 6-5, presenting a reasonable relative error.

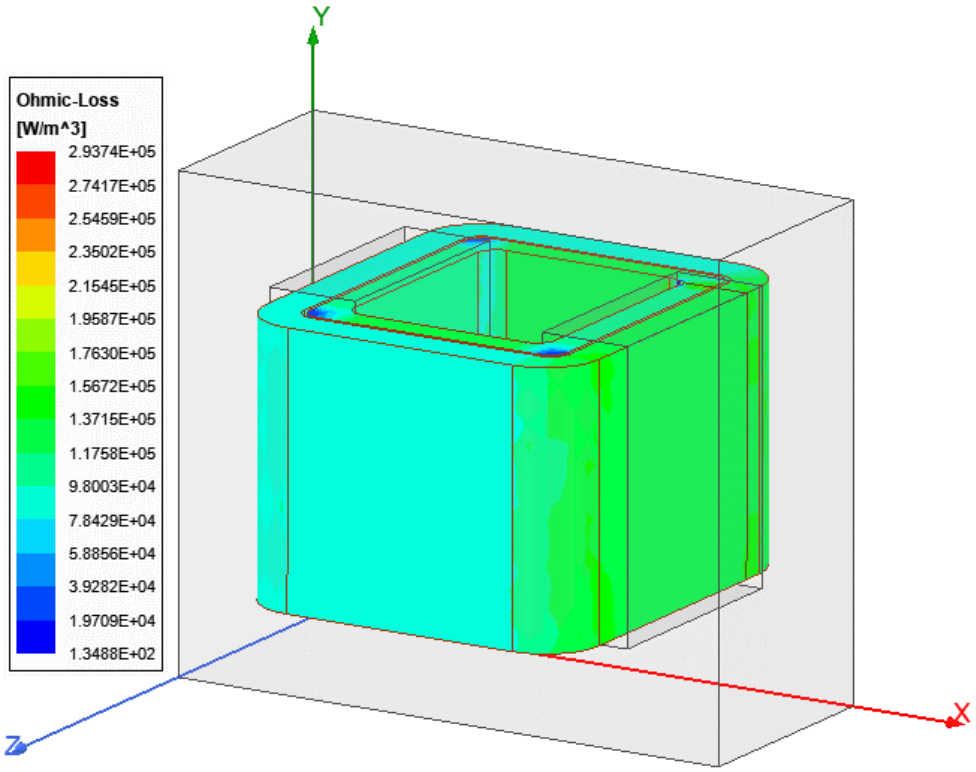

Figure 6-11. Resistive loss distribution by rated current operation.

Table 6-5. Comparative outputs, resistive loss.

	Resistive Loss (W) (Experimental test)	Resistive Loss (W) (FE analysis)	Relative error
Total resistive loss	41.00	40.05	2.32 %

Chapter 7

7 Conclusion

7.1 Work synthesis

This work proposed an analysis of single-phase transformer's losses by the finite element method, through the use of two dimensional approaches and frequency and time-varying domain. The focus of the project was to implement a useful computational model to model transformers behavior in different load conditions, to evaluate the accuracy of the method in losses prediction and verify the field distributions not easily to measurable in laboratorial tests.

First of all, the analytical project of magnetic parameters was designed with comparative purposes of magnetic magnitudes. To do so, it was necessary to develop the windings project, considering the physical characteristics of the transformer's core and wire gauge required to the rated currents. The reluctance network used to calculate the magnetic flux density around the middle path, regarding a 2D approach, provided outputs used to evaluate the simulation quality during the improvement of the model.

Second, the computational analyses started from a 2D magnetostatic approach able to verify the magnetic flux distribution considering only a planar domain, used to verify and edit the characteristics of the materials, which compose the machine components.

Sequentially, the previous model was projected considering three dimensions tested to predict the distribution and total value of the core and resistive losses in rating conditions. The outputs provided by the simulations were compared to experimental results from tests with a physical prototype. The values obtained by the experimental tests from open-circuit and short-circuit tests, which determine, respectively, the values of the core and resistive losses.

Finally, by time-varying simulations on the same model, it was possible to verify the electric magnitudes and evaluate if the transformer is working as it is expected by the magnetic project, and respecting the physics laws.

Therefore, after several analyses it is possible to conclude the efficiency of the method in electrical machines studies, since its use not only reduces the necessity of a large number of physical prototypes, but also allows the evaluation of the behavior of electric devices under extreme conditions, not always feasible, as three-phase power and distribution transformers experimental analyses.

7.2 Future work

There are several points that can help the development of future research in the field of electromagnetic analysis of electric machines assisted by the finite element method.

A relevant approach to be carried out is the modeling of high power three-phase transformers following the similar steps proposed by this work, which make it possible to verify the machine behavior in unusual activities.

By the use of the external circuit tool excitation, a promising field is the modeling of the winding, which allows simulations considering variating percentages of short-circuit faults in the windings.

References

[1] N. Ottosen and H. Petersson, *Introduction to the Finite Element Method*. Prentice Hall International, 1992.

[2] J. Jin, *The Finite Element Method in Electromagnetics*. New York: John Wiley & Sons, 1993.

[3] N. Bianchi, *Electrical Machine Analysis Using Finite Elements*. Taylor & Francis Group, 2005.

[4] I. Rezende, A. C. Azevedo, B. C. Carvalho, A. C. Delaiba, and J. C. de Oliveira, "Modelagem de transformadores trifásicos utilizando o método dos elementos finitos," pp. 1–4, 2005.

[5] P. Silvester and M. V. K. Chari, "Finite Element Solution of Saturable Magnetic Field Problems," *IEEE Trans. Power Appar. Syst.*, vol. PAS-89, no. 7, pp. 1642–1651, 1970, doi: 10.1109/TPAS.1970.292812.

[6] W. V. Calil, "Determinação de fator de correção para cálculo de perdas magnéticas em núcleos de transformadores de potência pelo método de elementos finitos," 2009.

[7] L. F. S. De Souza, F. M. Silva, I. N. Santos, and U. F. De Uberlândia, "Modelagem e análise eletromagnética de um transformador trifásico a seco através do método de elementos finitos," pp. 1–6, 2019.

[8] M. A. Plonus, *Applied Electromagnetics*. Singapore: McGraw-Hill, 1978.

[9] T. Demirdelen, "Optimal design and experimental validation long-lasting, low loss transformer for low power renewable energy system," *Energy Sources, Part A Recover. Util. Environ. Eff.*, vol. 41, no. 20, pp. 2534–2548, 2019, doi: 10.1080/15567036.2019.1637973.

[10] Y. Özüpak and M. S. Mamiş, "Realization of electromagnetic flux and thermal analyses of transformers by finite element method," *IEEJ Trans. Electr. Electron. Eng.*, vol. 14, no. 10, pp. 1478–1484, 2019, doi: 10.1002/tee.22966.

[11] J. A. Martinez and B. A. Mork, "Closure on 'Transformer modeling for low- and mid-frequency transients - A review,'" *IEEE Trans. Power Deliv.*, vol. 23, no. 3, p. 1697, 2008, doi: 10.1109/TPWRD.2008.924192.

[12] G. Kindermann, *Curto circuito*. Porto Alegre: Sagra Luzzatto, 1997.

[13] A. D. Theocharis, J. Milias-Argitis, and T. Zacharias, "Single-phase transformer model including magnetic hysteresis and eddy currents," *Springer*, vol. 90, no. 3, pp. 229–241, 2007, doi: 10.1007/s00202-007-0071-5.

[14] G. Bertotti, *Hysteresis in magnetism for physicists, materials scientists, and engineers*. Torino: Academic Press, 1998.

[15] K. Yamazaki, Y. Sato, M. Domenjoud, and L. Daniel, "Iron loss analysis of permanent-magnet machines by considering hysteresis loops affected by multi-axial stress," *IEEE Trans. Magn.*, vol. 56, no. 1, pp. 5–8, 2020, doi: 10.1109/TMAG.2019.2950727.

[16] N. Duan, W. Xu, Y. Li, S. Wang, Y. Guo, and J. Zhu, "Comparison of Limiting Loop Model and Elemental Operator Model for Magnetic Hysteresis of Ferromagnetic Materials," *IEEE Trans. Magn.*, vol. 53, no. 11, pp. 3–6, 2017, doi:

10.1109/TMAG.2017.2711265.

[17] C.-M. Ong, *Dynamic Simulation of Electric Machinery*. New Jersey: Prentice Hall, 1998.

[18] "ANSYS/Maxwell." 2019.

[19] A. Inc., "ANSYS Maxwell Training Manual : Maxwell postprocessig," pp. 1–21, 2013.

[20] Â. Ferreira, "Projecto de uma Máquina de Ímanes Permanentes de Fluxo Axial Orientado para os Sistemas de Conversão de Energia Eólica," 2011.

[21] A. Inc., "Maxwell 3D User's Guide," pp. 92–101, 2012.

[22] R. D. Cook, D. S. Malkus, M. E. Plesha, and R. J. Witt, *Concepts and applications of finite element analysis*, Fourth Edi. John Wiley & Sons, 2002.

[23] I. Koutromanos, *Fundamentals of Finite Element Analysis*. John Wiley & Sons, 2018.

[24] O. C. Zienkiewicz, R. L. Taylor, and J. Z. Zhu, *The Finite Element Method its Basis & Fundamentals*. McGraw-Hill, 2013.

[25] S. Lu and Y. Liu, "FEM analysis of DC saturation to assess transformer susceptibility to geomagnetically induced currents," *IEEE Trans. Power Deliv.*, vol. 8, no. 3, pp. 1367–1376, 1993, doi: 10.1109/61.252663.

[26] S. Liu, Z. Liu, and O. A. Mohammed, "FE-based modeling of single-phase distribution transformers with winding short circuit faults," *IEEE Trans. Magn.*, vol. 43, no. 4, pp. 1841–1844, 2007, doi: 10.1109/TMAG.2006.892302.

[27] S. Magdaleno-Adame, T. D. Kefalas, S. García-Martínez, and C. Perez-Rojas, "Electromagnetic finite element analysis of electrical steels combinations in lamination core steps of single-phase distribution transformers," *2017 IEEE Int. Autumn Meet. Power, Electron. Comput. ROPEC 2017*, vol. 2018-Janua, no. Ropec, pp. 1–5, 2017, doi: 10.1109/ROPEC.2017.8261585.

[28] P. Monk and Y. Zhang, "Finite Element Methods for Maxwell's Equations," *Encycl. Comput. Mech. Second Ed.*, pp. 1–20, 2017, doi: 10.1002/9781119176817.ecm2023.

[29] N. A. Demerdash and D. H. Gillott, "A new approach for determination of eddy current and flux penetration in nonlinear ferromagnetic materials," 1974.

[30] A. E. Chubykalo and R. Smirnov-Rueda, "Action at a distance as a full-value solution of Maxwell equations: The basis and application of the separated-potentials method," *Phys. Rev. E - Stat. Physics, Plasmas, Fluids, Relat. Interdiscip. Top.*, vol. 53, no. 5, pp. 5373–5381, 1996, doi: 10.1103/PhysRevE.53.5373.

[31] F. Assous, P. Degond, E. Heintze, A. Raviart, and J. Segre, "On a finite-element method for solving the three-dimensional maxwell equations," *Journal of Computational Physics*, vol. 109, no. 2. pp. 222–237, 1993, doi: 10.1006/jcph.1993.1214.

[32] M. Lax and D. F. Nelson, "Maxwell equations in material form," *J. Chem. Inf. Model.*, vol. 53, no. 9, pp. 1689–1699, 2018.

[33] A. Inc., "ANSYS Maxwell Training Manual: Static Magnetic Solvers," vol. 92, no. 3. p. 150, 2013.

[34] C. Multiphysics, "AC / DC Module User ' s Guide," *Comsol*, vol. 5.2. 2015.

[35] G. Bertotti, "General Properties of Power Losses in Soft Ferromagnetic Materials," *IEEE Xplore*, 1988.

[36] M. A. Mueller *et al.*, "Calculation of iron losses from time-stepped finite-element models

of cage induction machines," *IEE Conf. Publ.*, no. 412, pp. 88–92, 1995.

[37] Y. Zhan, "Stray loss of ac machines using time-stepped finite elements," University of Alberta, 2010.

[38] P. Vas, *Parameter Estimation, Condition Monitoring, and Diagnosis of Electrical Machines*. New York: Oxford University Press, 1993.

[39] P. Rasilo, E. Dlala, K. Fonteyn, J. Pippuri, A. Belahcen, and A. Arkkio, "Model of laminated ferromagnetic cores for loss prediction in electrical machines," *IET Electr. Power Appl.*, vol. 5, no. 7, pp. 580–588, 2011, doi: 10.1049/iet-epa.2010.0270.

[40] F. Deng, "An improved iron loss estimation for permanent magnet brushless machines," *IEEE Trans. Energy Convers.*, vol. 14, no. 4, pp. 1–5, 1999.

[41] H. C. Karmaker, "Stray losses in large synchronous machines," *IEEE Trans. Energy Convers.*, vol. 7, no. 1, pp. 148–153, 1992, doi: 10.1109/60.124554.

[42] IEC-60034-2-1, *Standard Rotating Electrical Machines*. 2007.

[43] C. I. Hubert, *Electric Machines: Theory, Operation, Applications, Adjustment, and Control*, 2nd ed. Prentice Hall, 2002.

[44] A. Inc., "ANSYS Maxwell Training Manual : Maxwell Transient Solvers," pp. 1–30, 2013.

[45] A. Inc., "Maxwell 2D User's Guide." pp. 2–4, 2011.

[46] A. Inc., "Maxwell 2D user's guide," *ANSYS Inc.*, pp. 92–101, 2010.

[47] A. Inc., "ANSYS Maxwell Training Manual : Meshing and Mesh Operations." pp. 1–20, 2013.

[48] Standard, "American Wire Gauge." .

Appendix A

Windings parameters

To the project of winding it was necessary to consider the rated currents of each coil, by to the rated voltages and power of the transformer. The calculation considered a room temperature of 20°C.

The electrical parameters requested to the transformer under analysis are shown in Table0A-1.

Table A-1. Project parameters

Parameters	
Power rating (VA)	1000
Frequency (Hz)	50
High voltage (V)	220
Low voltage (V)	110
HV: Rated current (A)	4.54
LV: Rated current (A)	9.09
Copper resistivity ρ (Ωm)	17×10^{-9}

Based on the AWG table the conductors selected to compose the high and low voltage windings are, respectively, AWG15 and AWG12, considering the rated currents. They are characterized as wire gauge, as presented in Table0A-2.

Table A-2. AWG characteristics. Adapted from [48]**.**

AWG number	**Diameter (mm)**	**Cross-sectional area (mm^2)**	**Resistance (Ω/Km)**	**Current intensity (A)**
12	2.053	3.31	5.13	9.5
15	1.450	1.65	10.3	4.8

Through the characteristics of the conductors (Table0A-2) and the Equation (A.1) the number or turns of LV winding are estimated, also considering the physical characteristics of the transformer's core.

$$R = \rho \frac{l}{A_c} \tag{A.1}$$

In Equation (A.1), l is the length of the wire, and A_c the cross-sectional area.

Finally, the number of turns of each winding and the value of the coils' resistance are shown in Table0A-3.

Table A-3. Windings parameters

Winding	Number of turns	Resistance (Ω)
High voltage	526	1.0
Low voltage	263	0.4

It is important to highlight that the transformer ratio defined by the rated voltages, was adjusted to 263/499 in the simulations as the physical prototype presented a transformer ratio of 220/116 V_{rms}.